Contents

About the cover: Scientists at LANSCE study image sequences of shock-wave interactions that are captured by proton radiographs. Definitive density gradients can be observed throughout the progression of growth.

Dr. Everet Beckner retired from the National Nuclear Security Administration of the Department of Energy April 29, 2005, after more than 40 years of dedicated public service to preserving and protecting the national security of the United States. Dr. Beckner is a fellow of the American Physical Society and a member of the American Association for the Advancement of Science. He has authored numerous papers on nuclear physics, plasma physics, and pulsed-power applications and reports on radiation effects in materials and components. The men and women of Los Alamos National Laboratory are indebted to Dr. Beckner for his unflagging support, which has been critical to our success over the years.

This issue of the *Nuclear Weapons Journal* is dedicated to Dr. Beckner.

Point *of* View

Los Alamos: An Innovator in the Nuclear Weapons Complex
David Beck
Associate Director, Acting
Weapons Engineering
and Manufacturing Directorate

In this time of uncertainty, why would someone choose a career at Los Alamos?

I say this: If you want to make a difference to national security and work on challenging, important issues that require a global perspective, come to Los Alamos. If you want to help make a better life for your fellow Americans using technology to solve tough problems in a multidisciplinary work environment, come to Los Alamos. If you want to collaborate with some of the world's top technologists using some of the most advanced computing and experimental facilities, come to Los Alamos. And if you want to spend the next 20–30 years making significant contributions in a place of major historical importance during a time in which your contributions will make a real difference, come to Los Alamos.

The Laboratory is now in a position to achieve even greater successes than those of the 6 decades in which we built our well-deserved reputation for science and technology excellence. The trials that we came through—from the reform of business practices to the safety/security work suspension—forged a Los Alamos National Laboratory that can provide the science and technology leadership the nation needs.

Some Laboratory employees complained that Washington and the media have mistreated the Laboratory. Any place with the reputation of Los Alamos is held to higher standards in safety and security, and rightly so. World-class science and engineering demand a rock-solid foundation of safety, security, and environmental excellence; an organization can claim to be world-class only if it has a world-class safety, security, and environmental record.

The role of managers is crucial. In any successful organization, management provides and articulates the mission, ensures that resources are adequate, removes barriers to achievement, and mentors and recognizes successes. At Los Alamos, managers and technical staff alike have a straightforward goal—solving technical problems in the interest of improved national security.

> **The United States needs the scientific foresight and capabilities of its national laboratories to provide national security.**

When the cold war ended, some thought the world would be a safer place. The harsh reality 15 years later is a dangerous and uncertain world. The US needs the scientific foresight and capabilities of its national laboratories, particularly Los Alamos, to provide a vision of national security and the technical leadership to realize that vision. Los Alamos has gone through its trials by fire and now is focused on science and engineering in the national interest, based on a solid foundation of security, safety, and environmental stewardship.

One overwhelmingly clear lesson that history teaches is that weakness reduces security. Recognizing that maintaining a responsive nuclear weapons infrastructure to support the stockpile could provide deterrence, the Department of Defense's 2001 Nuclear Posture Review defined our goals: assure our allies, deter adversaries, dissuade competition in nuclear armaments, and defeat our enemies. However, until we reach a national consensus about the specific role of nuclear deterrence in a long-term defense strategy,

The Physics of Ejecta

Scientists at the Los Alamos Neutron Science Center (LANSCE) are examining the physics of ejecta using proton radiography (pRad). Studying the shock waves that break out from a free (outside) surface of a metal, researchers are developing a theoretical model that may be used in weapons physics hydrodynamics codes.

The LANSCE accelerator produces multiple proton pulses that capture image sequences (proton radiographs) of dense materials under shock conditions. The high pressures and temperatures of shock waves can (1) leave the material in the original solid state, (2) cause metals and other materials to melt, or (3) produce a mixed liquid-solid phase (also called "condition" or "regime") instead of a purely liquid state. Mixed-phase materials (i.e., solid particles in a liquid suspension) may behave as a viscous liquid in which viscosity increases with the number of solid particles in suspension.

Experimental configuration. Positioned between the tin target and an HE source, the aluminum flyer impacts the target after the HE detonates. Using pRad techniques, researchers photograph and measure the effect of shock waves propagated at the interface of the tin target and the aluminum flyer.

Liquid Regime

Instabilities in the liquid regime often are physically described and characterized by bubbles and spikes. Using 3-D bubble merger, spike distribution, and breakup theories, a team from the Dynamic Experimentation, Physics, and Applied Physics Divisions is developing a series of coupled equations to describe the bubble and spike phenomena and determine particle-size distribution for ejecta as a function of time. These contributions to theory may be used to fill gaps in experimental data and to enhance hydrodynamics simulations.

pRad Experiment

When materials are shocked, their surfaces may become unstable as they move into the surrounding medium. These unstable processes cause coherent (stable) structures to appear within an otherwise incoherent (unstable) background. In liquid metals, the effects of significant surface tension and viscosity decrease the growth rate of instabilities. To ascertain the effectiveness of the surface tension model in their hydrodynamics code (a 3-D Eulerian code that includes surface tension) and the error from the code's inability to model viscosity, the researchers conducted a 2-D, Richtmyer-Meshkov (RM) instability experiment using shock-liquefied tin. The experiment established a baseline in a relevant regime so, that they could compare their results with existing analytical theories, simulations, and experiments before conducting more complex 3-D RM instability simulations with the Eulerian code to study ejecta.

Although extensive experiments have investigated the 2-D, single-mode growth of RM instabilities, the work typically involved experiments with gases or plasmas. Such experiments do not account for the complexity of surface tension interactions or the effects of viscosity on RM instability growth at the interface of a liquid metal as it ejects
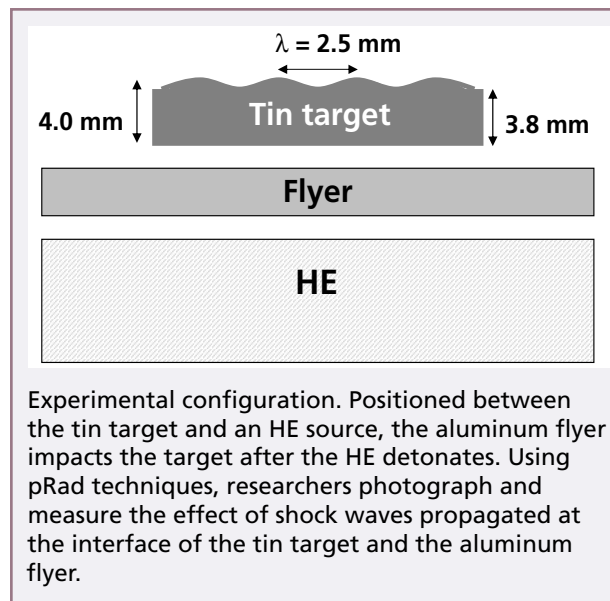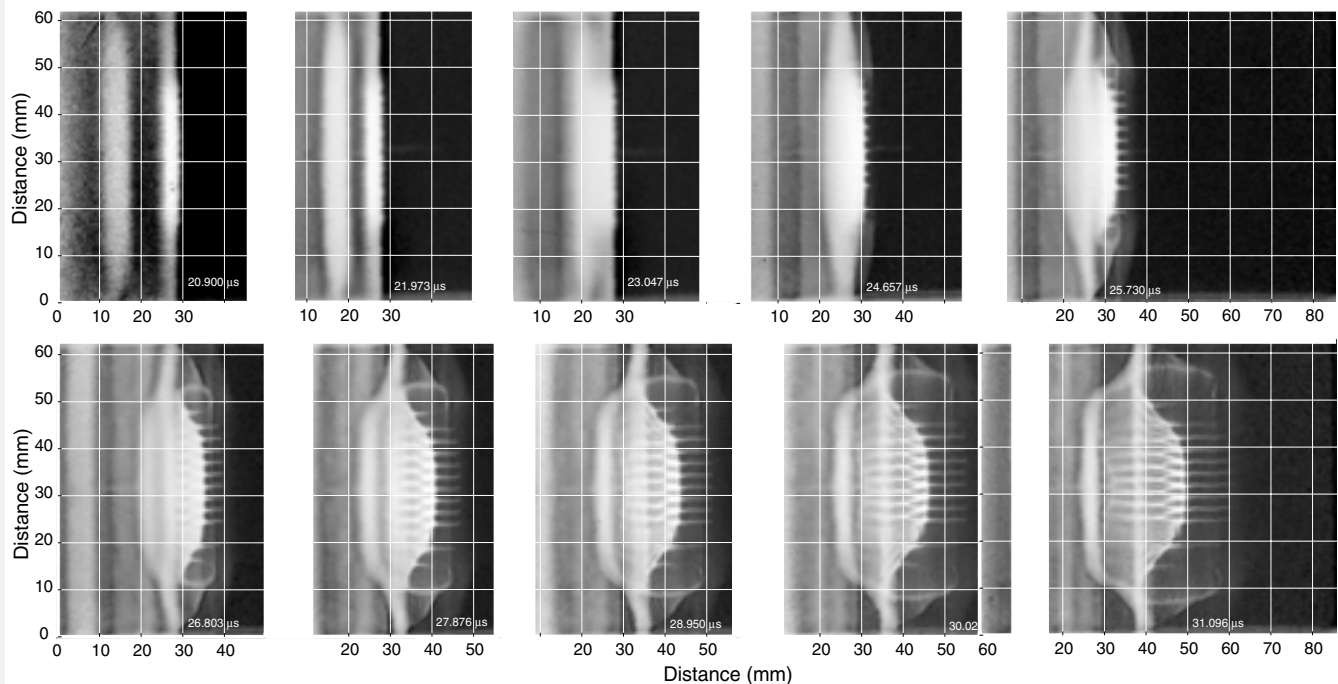
Series of images from a nine-frame camera. In the first (top left) frame, the flyer moves toward the target residing in its plastic frame. Target impact has occurred by the second frame, to the extent that the flyer-target system has become compressed; instability growth is well under way by the third frame and progresses throughout the remaining images. Analysis of further images showed that the velocity of the instability tips was ~4.5 mm/μs. Times from detonation are (top, left to right) 20.90, 21.97, 23.05, 24.66, and 25.73 and (bottom, left to right) 26.80, 27.88, 28.95, 30.02, and 31.10 μs.

particles ("ejecta"). Although these effects may not significantly affect RM instability growth, they are of great importance to ejecta production because (1) the Rayleigh instability is a surface-tension instability, (2) liquid metals have high viscosities, and (3) the effective viscosity of mixed-phase materials may be much higher than that of any completely pure, i.e., liquid (free of solid particles), substance.

LANSCE scientists use pRad ejecta images to study shock wave interactions.

In the experiment, tin targets were shocked up to a pressure of ~650 kb (beyond the melt-on-shock pressure of ~600 kb), producing the resultant instability formation. To maximize the planarity or "flatness" of the shock wave propagated through the target, a Forest flyer package was used in which high-explosive (HE) detonation propelled an aluminum flyer over a distance of 22 mm to impact a 40-mm-diameter tin target. The impact-driven shock plane wave propagated through the target at a velocity of ~4.93 mm/μs and unloaded effectively at zero pressure on the opposite (free) side, which had been machined with a "single-mode" sinusoidal contour to the following total amplitude (A_T):

$$A_T(\text{mm}) = 3.8 + 2A\cos\left[\frac{2\pi x}{\lambda}\right],$$

where A = 0.2 mm, the maximum deviation from the amplitude mean; λ = 2.5 mm, the sinusoidal wavelength; and x is the perpendicular position along the target's diameter.

To minimize motion blur, the pulse width of the protons used to generate each image frame was 40 ns. Images were acquired at approximately 0.5-μs intervals, beginning before the flyer impact and continuing for approximately 20 μs afterwards. This time range provided an opportunity to

- determine flyer velocity (~4.5 mm/μs before impact),

- determine whether the flyer spalled before impact (a phenomenon undesirable for optimal shock propagation), and

- observe instability growth.

A striking view of the instability growth, acquired at ~31 μs after detonation initiated (~9 μs after the shock wave initially traversed the tin target), showed various manifestations of shock wave interactions; the prominent rising spike tips demonstrated the "first excited mode" arising from the initial unloading interaction of the shock wave with the target's minimum in the sinusoidal surface. A reflection from the tin-vacuum interface extended to the indistinct aluminum (flyer)-tin interface, and those reflected shock propagations extended in reverse still further into the aluminum from the tin.

A "second excited mode," arising from a secondary shock wave or rarefaction wave unloading again at the tin-vacuum interface, began to appear in the interstices of the largest spikes where the target surface had inverted and troughs had formed. Secondary spikes emerged from a uniform ejecta cloud of tin particles, which formed at the tin-vacuum interface. Edge effects apparent at the aluminum
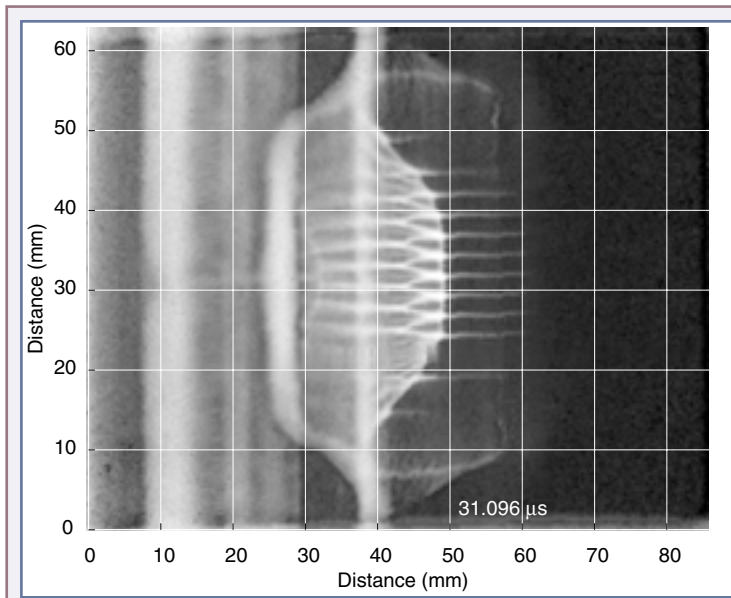
Instability growth at 31.096 μs after detonation. Shock-wave interactions are apparent in the prominent rising spike tips (the "first excited mode") as the shock wave encounters the target's sinusoidal surface. Definitive density gradients can be observed throughout the progression of growth. A reflection from the tin surface extends back to the indistinct aluminum-tin boundary, continuing still further to the other side of the aluminum flyer. The "second excited mode," arising from a secondary shock wave–interface encounter, appears in the interstices of the primary prominences (spikes) where the surface has inverted and troughs have formed. The secondary spikes emerge from a uniform ejecta cloud that formed at the tin-vacuum interface. Edge effects are apparent where the aluminum interfaces with the target's plastic frame, slightly occluding much of the view of the spikes, rendering a refraction effect near the top of the rising spikes.

interface with the target frame slightly occluded much of the view of the spikes, rendering what appeared to be a type of refraction effect near the top of the rising spikes.

Additional Experiments

In addition to the RM-instability experiment, the Los Alamos team is pursuing a second series of tin experiments in support of their ejecta theory. The team is acquiring data on the total amount of metal particulate ejected from the surface of well-characterized tin disks as a function of surface roughness and shock strength. These data will enhance the database needed to validate an ejecta source model the team will develop for the second series of experiments. NWJ

Points of contact:
W. T. Buttler, 665-1071, buttler@lanl.gov
W. S. Vogan, 665-1711, vogan@lanl.gov

Other contributors to this project include the proton radiography team, L. Day, J. E. Hammerberg, R. S. Hixson, G. Hogan, F. Mariam, F. E. Merrill, K. B. Morley, C. Morris, P. Nedrow, D. L. Preston, K. P. Prestridge, A. Saunders, C. Schwartz, D. Shampine, D. P. Smitherman, and M. D. Wilke.

Theory of Ejecta

When a shock wave unloads at (breaks out of) the free (outside) surface of a metal, small particles of material are ejected from the surface. Los Alamos scientists are exploring the physics of ejecta in order to develop a theoretical model for hydrodynamics codes.

The ejecta distribution function, M, is given by

$$M(D,v,P,S,\hat{n} \bullet \hat{u}, n_S) = M_j(P,S,\hat{n} \bullet \hat{u}, n_S)f_1(D)f_2(v).$$

D and v are particle diameters (assuming spherical particles) and velocities, while f_1 and f_2 are particle and velocity distribution functions for these quantities. Integrals of the distribution functions are normalized to 1. The quantity M_j is the mass ejected and is assumed to be a function of the shock pressure P, entropy S, with obliquity represented as the dot product of the unit vector normal to the surface $\hat{n}$ with the unit shock velocity vector $\hat{u}$, and the surface roughness distribution function n_S. In the future, the function may include grain effects, as well.

Experimental ejecta data are derived from two classes of diagnostics: those that measure mass-related properties (e.g., Asay foils, piezoelectric sensors, x-ray attenuation techniques) and those that measure size-related properties (e.g., holography).

Asay foils, piezoelectric data, and radiography correlate the total mass ejected and velocity but give no quantitative information on particle-size distribution. The velocity distribution $f_2(v)$ may be obtained experimentally from these diagnostics and appears to be an exponentially decaying function of velocity, with the slowest velocity corresponding to the free surface of the metal.

Holography provides particle-size distribution correlated with the particle-velocity distribution but is limited to a spatial resolution of 1 to 2 µm and records only the very fastest ejecta particles. Holography may be used to determine $f_1(D)$.

Before an ejecta distribution function can be calculated, the total amount of ejecta thrown from the free surface must be determined. The amount of ejecta can be considered directly proportional to the defect volume of the scratches on the surface of a metal, with the proportionality constant, R, as the jetting factor (a function of defect geometry). Early (1970s) experiments and simulations to determine the jetting factor considered only solid materials. However, when a shock melts its host material to form a liquid, a much larger quantity of matter is ejected.

Current experimental data do not answer the following questions:

• What is the particle distribution below the holographic spatial limit?

• What is the particle distribution below the holographic velocity limit?

• How does one predict R when the material is molten?

To answer these questions, Los Alamos will conduct 3-D simulations of ejecta with a Eulerian code and is pursuing a theoretical model for the liquid case.

Although many processes occur at the interface during ejecta production, the most significant is the Richtmyer-Meshkov (RM) instability. The 3-D simulations can direct theoretical work by addressing many issues, such as whether ejecta forms before or after a dominant, coherent bubble-spike mode arises out of the otherwise incoherent background. Comparing code results to the simple RM instability experiment with liquid tin gives confidence that the code is directing researchers in the proper theoretical directions.

Points of contact:
D. P. Smitherman, 667-0548, dps@lanl.gov
W. T. Buttler, 665-1071, buttler@lanl.gov

Other contributors to this project are D. L. Preston and J. E. Hammerberg.

Achieving Predictive Capability for Laser Plasma Interaction

Trident is LANL's multipurpose plasma physics laboratory used to conduct experiments that require high-intensity, laser-light pulses.

Trident is a "user" facility: both LANL and visiting scientists use Trident's unique capabilities to develop diagnostic instrumentation and fabrication technologies, advance simulation capabilities, and investigate relevant issues. Trident users apply these capabilities to programs of national importance, such as the achievement of ignition—the fusion of heavy hydrogen—in the Inertial Confinement Fusion (ICF) Program and to answer major questions about the absorption of laser light as it arrives at its target.

Supporting research at Lawrence Livermore National Laboratory's (LLNL) National Ignition Facility (NIF), LANL's Laser Plasma Interaction (LPI) Theory Team uses Trident's unique capabilities to study—and eventually predict—where and how NIF laser light is absorbed when it strikes a target. This work is challenging because each laser beam is composed of thousands of random speckles (localized regions of intensity maxima), which change in space and time. Because a typical speckle is small (approximately 200 μm by a few micrometers) and can be regarded as an irreducible element of a laser beam, current Trident studies focus on a single speckle. Our primary simulation tools for this study are particle-in-cell (PIC) and reduced particle-in-cell (RPIC) codes, which solve Maxwell's equations and Newton's equation for individual particles. Trident experiments validate the use of these tools.

At LANL, our theory team follows two approaches that can implement these single-speckle research results into multispeckle simulations:

- factoring results into the 3-D paraxial code pF3D using pF3D as a predictive tool and

- inputting pF3D fields into a statistical simulation code.

Reflectivity rises in plasmas and then saturates at a higher level as laser-speckle intensity increases.

Single-Speckle Simulations

Recognizing that a single speckle in a laser beam can be considered a basic building block, we devised Trident laser experiments that mimic a single NIF speckle. For these experiments, Trident's interaction laser is set at 527 nm, striking a uniform plasma at 3% to 10% of critical density; a Thomson scattering probe beam is set at 351 nm. These single-hot-spot experiments are well characterized and well diagnosed and can be modeled with no simplifying assumptions. Thus, our theory effort focuses on understanding and predicting the characteristics of Trident experiments.

Our simulations and experiments show the dominance of two nonlinear processes for NIF parameters: stimulated Raman scattering (SRS) and stimulated Brillouin scattering (SBS). SRS is the decay of incident light wave into a scattered light wave and an electron plasma wave. SBS is the decay of incident light wave into a scattered light wave and
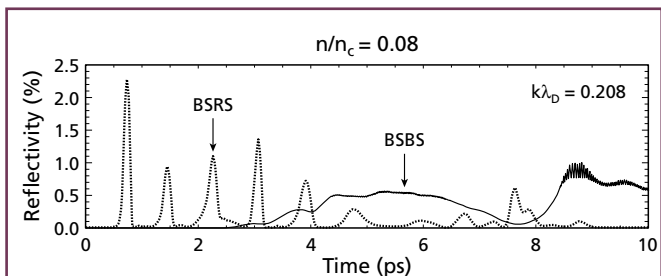
Percent of reflected laser-light caused by BSRS and BSBS as a function of time. Note that BSRS is greatly reduced in the presence of BSBS; they seem to be anticorrelated. Peak speckle intensity is 4×10^{15} W/cm^2.

an ion acoustic wave. SRS and SBS processes are capable of moving backward (back toward the incident light) and forward (in the direction of the incident light). Here we discuss only backward SRS (BSRS) and backward SBS (BSBS).

RPIC simulations reveal the interplay between BSRS and BSBS, which can be plotted as a function of time. BSRS pulsates at regular intervals and is suppressed as BSBS develops. This behavior has been observed consistently in simulations, predicted by theory, and indicated in experiments.
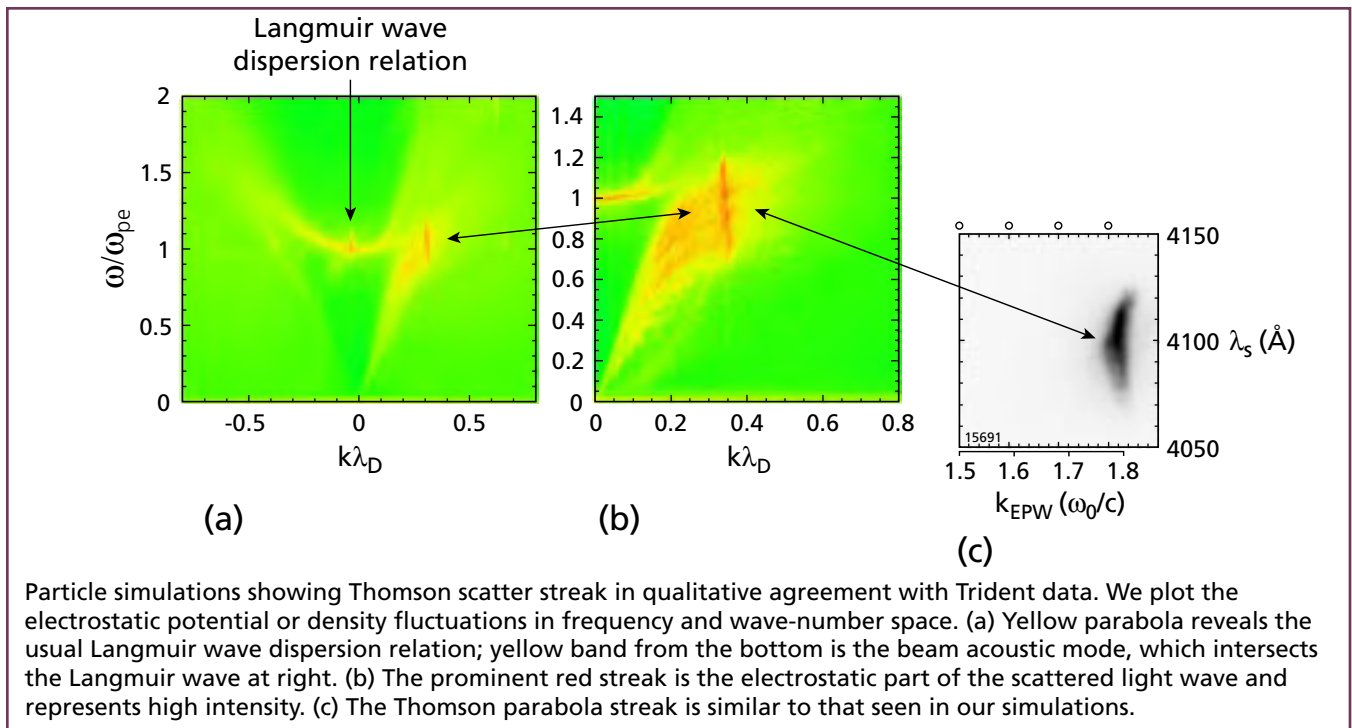
We now have significant capability for modeling BSRS in a single speckle and we have predicted the following processes:

• transition from fluid to kinetic regime for NIF-like parameters,

• Langmuir decay instability (LDI) cascade,

• large scatter for NIF parameters in kinetic regime,

• frequency streak of Thomson scatter spectrum in experiments, and

• sharp, nonlinear BSRS onset from small to large scattering (or "cliff").

Although we have not achieved full quantitative agreement in all cases, we have achieved very good qualitative agreement in our comparisons with Trident experiments.

For small $k\lambda_D$, where k is the Langmuir wave number and λ_D is the electron Debye length, BSRS saturates by fluid processes. In particular, the excited Langmuir wave can decay into another Langmuir wave and an ion acoustic wave, or LDI. This Langmuir wave in the LDI process can decay repetitively into additional Langmuir and ion acoustic waves, producing an LDI cascade. This cascading behavior has been observed in both plasma simulations and experiments.

For large $k\lambda_D$ (for example, greater than approximately 0.3), saturation occurs by electron trapping or by kinetic effects: the nonlinear Langmuir wave spectrum is narrow in k and grows until a significant number of particles are trapped. We studied the transition from small to large $k\lambda_D$ by carrying out PIC simulations for Trident parameters. We calculated Thomson scattering electron density fluctuations and did a Fourier analysis in space and time. Our experiments show a spectrum that is narrow in k and broad in the corresponding frequency of the wave (ω), much like our simulations. This agreement between simulations and experimental results

Particle simulations showing Thomson scatter streak in qualitative agreement with Trident data. We plot the electrostatic potential or density fluctuations in frequency and wave-number space. (a) Yellow parabola reveals the usual Langmuir wave dispersion relation; yellow band from the bottom is the beam acoustic mode, which intersects the Langmuir wave at right. (b) The prominent red streak is the electrostatic part of the scattered light wave and represents high intensity. (c) The Thomson parabola streak is similar to that seen in our simulations.
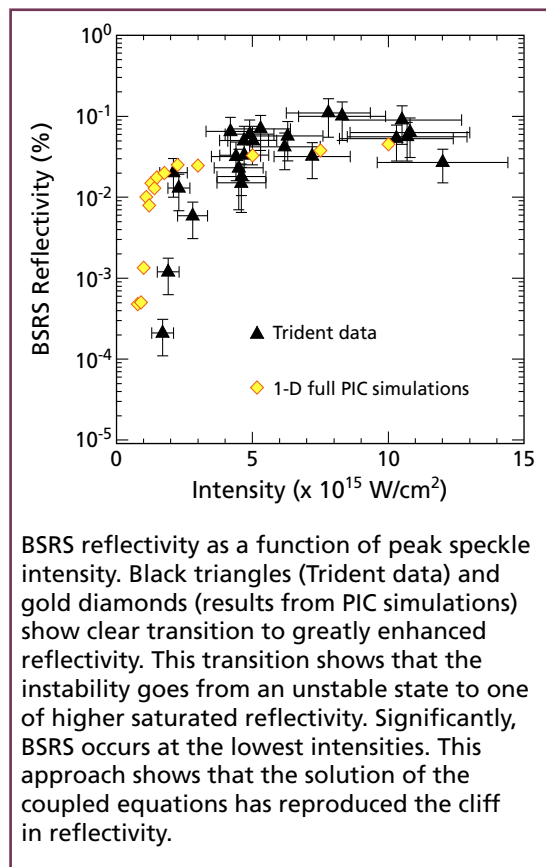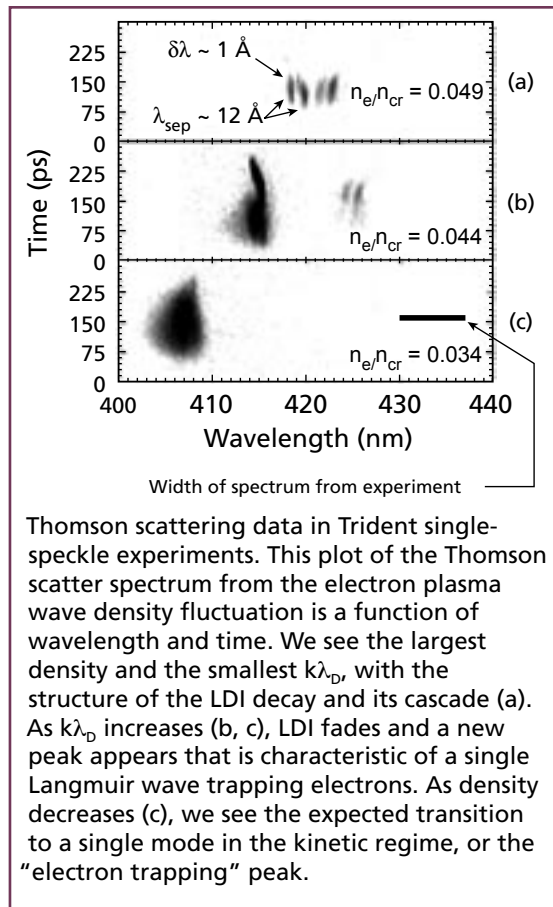
enhances our confidence in our simulations.

Trident experiments also have shown the transition in saturation from wave-wave (LDI or fluid) to wave-particle (kinetic) saturation. Our theory predicts this transition in the Trident experiments, differing in transition $k\lambda_D$ values.

A potentially very important result for NIF is seen both in our Trident experiments and in our simulations when we plot reflectivity from BSRS as a function of peak speckle intensity. At the lowest intensities, we see BSRS saturation; at some critical intensity, however, reflectivity rises suddenly and then saturates at a much higher level as intensity increases. This sudden onset of reflectivity at a critical intensity suggests the possibility that NIF can operate below this critical intensity without unacceptable backscatter.

Summary
We use our single-speckle results to attempt to understand multispeckle issues for single laser beams. Our primary approach is to put our results into fluid equations that can be implemented in a 3-D laser fluid code (the LLNL paraxial code pF3D). This code incorporates calculations for the thousands of laser speckles in each NIF laser beam, resolving BSRS issues for each speckle. We put the BSRS single-speckle results into a model that uses coupled fluid equations for the incident

Width of spectrum from experiment

Thomson scattering data in Trident single-speckle experiments. This plot of the Thomson scatter spectrum from the electron plasma wave density fluctuation is a function of wavelength and time. We see the largest density and the smallest $k\lambda_D$, with the structure of the LDI decay and its cascade (a). As $k\lambda_D$ increases (b, c), LDI fades and a new peak appears that is characteristic of a single Langmuir wave trapping electrons. As density decreases (c), we see the expected transition to a single mode in the kinetic regime, or the "electron trapping" peak.

BSRS reflectivity as a function of peak speckle intensity. Black triangles (Trident data) and gold diamonds (results from PIC simulations) show clear transition to greatly enhanced reflectivity. This transition shows that the instability goes from an unstable state to one of higher saturated reflectivity. Significantly, BSRS occurs at the lowest intensities. This approach shows that the solution of the coupled equations has reproduced the cliff in reflectivity.

laser, scattered light wave, and electron plasma wave. We include nonlinear kinetic effects on the electron plasma wave because they limit the size of the plasma wave and produce a corresponding limitation on the scattered light. We are now exploring ways to implement our 1-D simulation results in pF3D.

With 1-D PIC and RPIC simulations of a single-laser speckle, we have obtained good qualitative agreement with single-speckle Trident experiments. That is, even though the experiment had 3-D effects and flow, with 1-D codes we could predict the observed nonlinear physics: transition from fluid to kinetic regime for NIF-like parameters, LDI cascade, large scatter for NIF parameters in kinetic regime, frequency streak of Thomson scatter spectrum in experiments, and Raman nonlinear cliff.
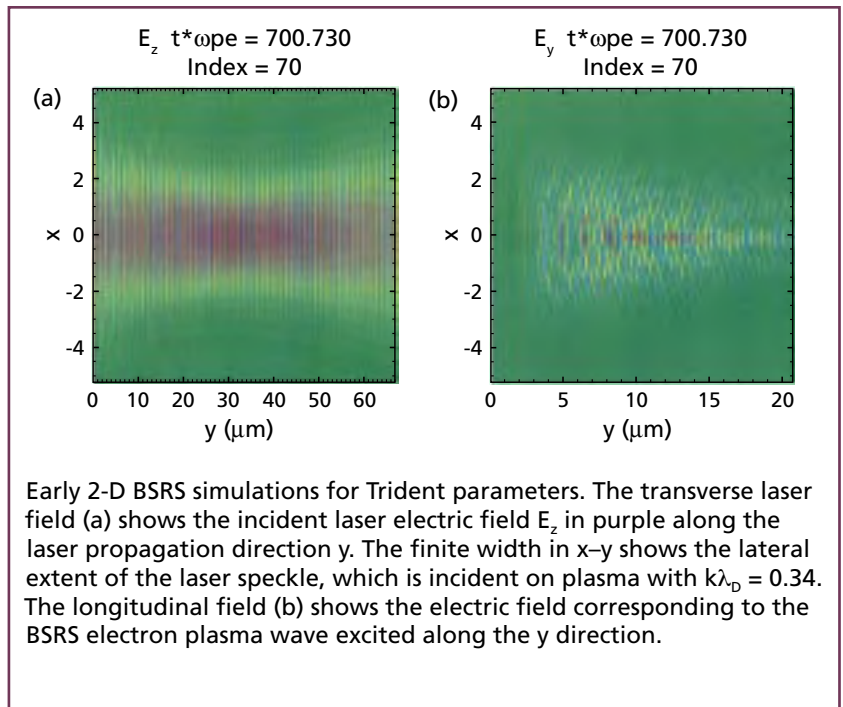
However, from a modeling perspective we must question whether any multidimensional effects occur. Is BSRS primarily a 1-D, nonlinear phenomenon? Does proper multidimensional treatment of the light and electrons moving transversely from the electron plasma wave significantly change results? Should we see or expect additional physical effects such as self-focusing of the speckle?

To address these issues, we initiated 2-D PIC simulations. Although it is premature to say whether the simulation will remain 1-D, the significance of our results is that the electron plasma wave is largely 1-D with limited 2-D structure. Subsequent Trident work will help us resolve this issue. NWJ

Point of contact:
Joe Kindel, 667-7299, jkindel@lanl.gov

The plasma physics team for this work included Brian J. Albright, Bandel Bezzerides, Bill Daughton, Evan S. Dodd, Don DuBois, John Kline, David Montgomery, Mark Schmitt, Hoanh Vu, and Lin Yin.

E_z t*ωpe = 700.730
Index = 70

E_y t*ωpe = 700.730
Index = 70

Early 2-D BSRS simulations for Trident parameters. The transverse laser field (a) shows the incident laser electric field E_z in purple along the laser propagation direction y. The finite width in x–y shows the lateral extent of the laser speckle, which is incident on plasma with $k\lambda_D = 0.34$. The longitudinal field (b) shows the electric field corresponding to the BSRS electron plasma wave excited along the y direction.

DEFINITIONS

Brillouin scattering—Light scattering by acoustic phonons.

cliff—Sharp, nonlinear BSRS onset from small to large scattering.

Debye length—Shielding distance; characteristic distance in a plasma beyond which the electric field in a charged particle is shielded by particles having charges of the opposite sign.

Fourier analysis—Analysis of a periodic function into a sum of simple sinusoidal components.

incident light—Light that emanates from a laser and falls on a surface.

ion acoustic wave—Low-frequency, longitudinal electrostatic wave that propagates because of variations in the plasma density; involves both ions and electrons.

Langmuir decay instability—Process in which a Langmuir wave loses its energy by exciting both a backward-propagating Langmuir wave and a forward-going ion acoustic wave.

Langmuir wave—High-frequency, longitudinal electrostatic wave that propagates in a plasma because of variations in the plasma's density; involves only electrons.

LDI cascade—Langmuir wave in a repeating LDI process.

Maxwell's equations—Four differential equations that summarize classical properties of electromagnetic fields.

Newton's equation (of motion)—Newton's laws of motion expressed in the form of mathematical equations.

speckle—Localized maximum in light wave intensity.

Thomson scattering—Scattering of electromagnetic radiation by free or loosely bound charged particles.

Polymer and Foam Equation of State Theory and Model Development

Polymers and polymeric foams have several important properties in common with high explosives (HE). Like HE, polymers are organic solids or liquids, they decompose rapidly under shock conditions, and the decomposition products are a mixture of molecular fluids and solids at high pressure and temperature. The distinction between polymers and HE is that polymers do not release enough energy to propagate the detonation shock without support. On the other hand, an explosive-driven polymer configuration easily produces enough shock heating and pressure to cause fast reaction and make the polymer decomposition products look a lot like detonation products. Indeed, that was the starting point for developing theoretical modeling of the equation of state (EOS) of polymers and foams.


The theoretical model for decomposed polymer starts from an EOS developed for detonation products.


Some of the qualitative behaviors of polymers under shock conditions were previously well established from experimental data. For example, an inert plate can be launched to high velocity with either an explosive driver or a gas gun. When this plate strikes a sample, a shock wave is sent through the sample with a constant thermodynamic state and a constant particle velocity behind the shock. The set of states that can be reached in a single shock is called the Hugoniot. The pressure, density, and energy in the shocked state can be determined by measuring the shock velocity and particle velocity along with hydrodynamic constraints from conservation of mass, momentum, and energy.

The Hugoniot data for polystyrene show clear signs of a large volume change. For inert materials this could be the signal of a phase transition. In reactive materials, such as polymers, the change in volume is due to a significant difference in the EOS for reactants and products. The shock velocity versus particle velocity graph shows a typical linear behavior with a slope at low particle velocity. Then, at a particle velocity of around 3 km/s, there is a flat section with zero slope, followed by another straight-line segment with a different slope. These features are characteristic of a two-wave structure in the region
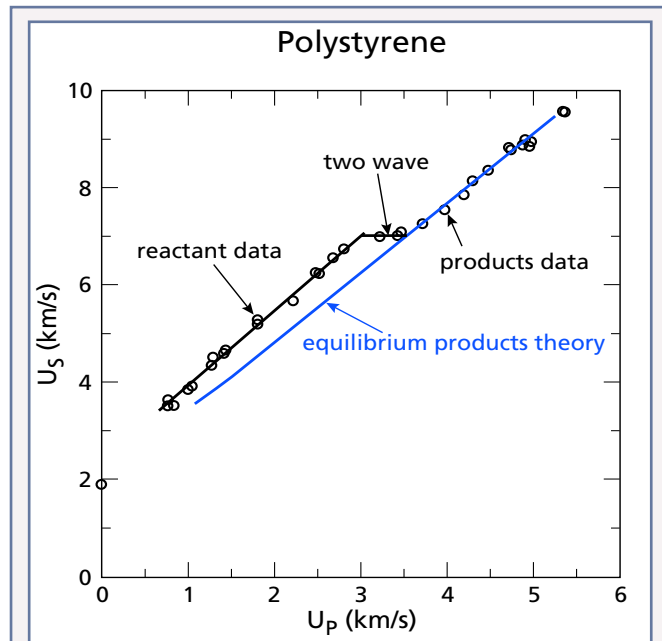
Polystyrene

U_S (shock velocity) versus U_P (particle velocity) for polystyrene. The three straight lines show reactant, two-wave structure, and products as the particle velocity increases. The linear U_S-U_P behavior for the reactant is common to most inert materials. The constant shock velocity region is similar to that found in phase changes in iron. The initial wave propagates at the shock velocity corresponding to the transition pressure in the initial material. A second wave follows at the final state for the product material and gives the impedance match that shows up in the particle velocity measurement. Once the pressure is high enough to give a faster shock velocity, the single shock behavior resumes with a near linear U_S-U_P behavior. Note that recovery experiments below the transition pressure show samples that are still polymer. Above the transition pressure, soot and gases are recovered.
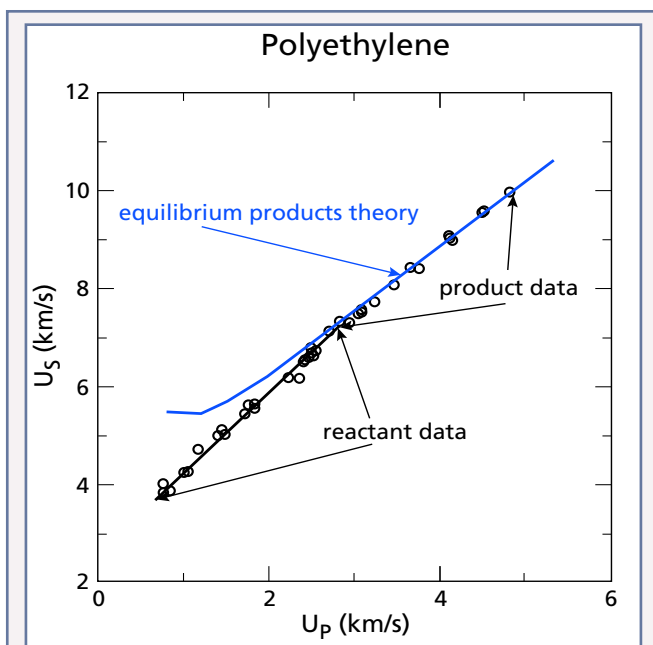
Polyethylene

U_S versus U_P data (symbol O) for polyethylene. A straight line is drawn through the lower portion of the data as a fit to the inert material. The theoretical model for equilibrium products (blue line) agrees very well with the data where the slope has changed. In this case, the constant shock velocity region is very small or missing due to a small change in volume with the transition to products. Recovery experiments show polymer from shocks below the slope change. At higher velocities, soot and gases are recovered in agreement with the assumption of an equilibrium products EOS.

of flat slope. Under these circumstances, a single shock wave solution is not allowed. Instead, the shock runs at a fixed velocity corresponding to the point on the Hugoniot where a rapid reaction begins. A second shock jumps to a state in the products that matches the particle velocity in the flyer plate. Other polymers, such as polyethylene, have a slope change but no obvious flat region, a pattern corresponding to a small volume change. In this case, the products EOS is similar to the reactants EOS. The reactant and product EOSs vary in different ways with composition. Compositions for which the reactant and product EOSs are nearly the same result from an accident of this variation.

The issue of the cause of these features was settled in the 1980s by recovery experiments at Los Alamos National Laboratory designed to examine the condition of samples subjected to a pressure shock. Samples shocked in the lower particle velocity region of the velocity comparison graph were still the original

polymer, more or less. Higher particle velocities, in the two-wave region or in the slope change region of the graph, produced decomposition products—soot and gases—that were found to be mixtures of mainly hydrogen (H_2) and methane (CH_4). These results indicate that volume change and/or slope change corresponded to a change from reactant to products.

The theoretical model for decomposed polymers starts from an EOS developed for detonation products. In the calculation of thermodynamic properties, the most important contribution is determined from the intermolecular potential energy. This interaction is well approximated by contributions from a spherically symmetric pair potential chosen to reproduce the contributions of the full potential energy, including angular dependence. The thermodynamics for that potential is given by a thermodynamic perturbation theory shown to be accurate for the relevant high pressures and temperatures. The potentials were chosen to give a good match to available data and higher-level calculations, both for a single molecular fluid and for the mixtures of fluids occurring in actual detonation products. Further complications included in the EOS treatment are carbon clusters, including the possibility of surface chemistry. The equilibrium chemical composition is then readily determined from the full mixture EOS (by minimization of the Gibbs free energy as a function of molecular species concentrations).

Polymers are very similar to HE in that, under shock conditions of sufficient strength, the initial polymer material decomposes to a mixture of molecular fluids (N_2, H_2O, CO, CO_2, H_2, CH_4, etc.) and sometimes solids (C, SiO_2, etc.). Although the energy released in the decomposition of polymers is small compared to HE energy release, the final state can still be at high temperature due to shock heating. In the case of foams, the shock heating is quite substantial, and the resulting temperature is often in the same range as for HE.

The difference between polymer products and HE products is primarily in the concentration of product species and not in the type. Consequently, the same theoretical methods for obtaining the EOS

are applied to both. Only minor modifications were required to apply the HE theoretical method to polymer products. Furthermore, only a limited amount of experimental calibration was needed to make the jump from HE to polymers. In particular, the concentrations of H_2 and CH_4 are high for polymer products and low for HE products. Minor adjustments in the potential for these two species have led to a polymer EOS in very good agreement with previous experimental data on an initial set of polymers, including polystyrene and polyethylene.

The products EOS for polymers was nearly predictive without adjustment due to features of typical compositions. The HE products EOS is very sensitive to the relative concentrations of C, CO, and CO_2 in the products determined by chemical equilibrium (where different concentrations can change the energy release by 20% or more). Polymers typically contain little or no oxygen (which preferably forms H_2O), and hence sensitivity to that equilibration disappears. Likewise, the relatively large amount of carbon leads to carbon clusters sufficiently large to be accurately treated as bulk without complications of surface effects.

The reactants are treated like inert materials with a simple fit to the data. A treatment of polymers is incomplete without at least an estimate of the conditions required for decomposition. The reaction rate of decomposition is expected to be very sensitive to the temperature. A simple limiting approximation is used: the polymer can be accurately approximated as either inert reactant or equilibrium products, depending on the state. This appears to be the case for some common polymers such as polystyrene. The transition to products seems to occur at about the same particle velocity (around 3 km/s) for such polymers and consequently at about the same specific internal energy added by the shock. The unreacted EOS model shows that the temperature in a typical polymer is well over 1000 K at that particle velocity. At that kind of temperature, organic molecules tend to react rapidly.

A variety of polymers and foams are of interest for various applications. We will focus here on a particular example, the foam S5370, that illustrates the process. (The related foam LK3626 has essentially

the same composition and should be identical in behavior except at very low pressures where material properties are important). The primary constituent of S5370 is polydimethylsiloxane (PDMS), which has the formula $CH_3\text{-}Si(CH_3)_2\text{-}[O\text{-}Si(CH_3)_2]_n\text{-}CH_3$, where the term in brackets repeats n times in the polymer chain. Similar silicon compounds are also included to a lesser extent, plus SiO_2 (which is added as filler to link the polymer chains together). The product composition in chemical equilibrium includes silicon compounds that are not a part of the set of usual products of HE or of the polymers in the initial comparison set. The new silicon products are dominated by two solid species: SiO_2 because of its very negative heat of formation (which relates the enthalpy of a compound to that of its constituent elements) and SiC because there is not enough oxygen to react with all of the silicon. Consequently, the energy release is sensitive to the amount of available oxygen. Static and shock data were used to calibrate the EOSs for these new additions to the product EOS code. For a polymer
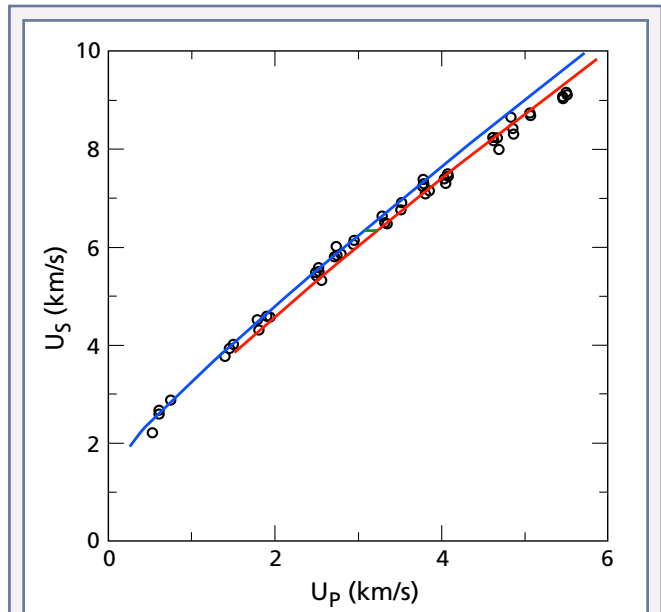
U_S versus U_P data (O) for Sylgard 184. The equilibrium products theoretical model (red line) is in excellent agreement with the data. A best fit of the cold curve to the lower portion of the data is given by the blue line. An estimate of the transition is given by the short green line that indicates the two-wave structure region. With the addition of silicon to the composition, the theoretical model is still valid. The transition still occurs around a particle velocity of 3 km/s, which gives a shock driven energy deposition of 4.5 kJ/g, almost up to the heat of explosion for TNT.
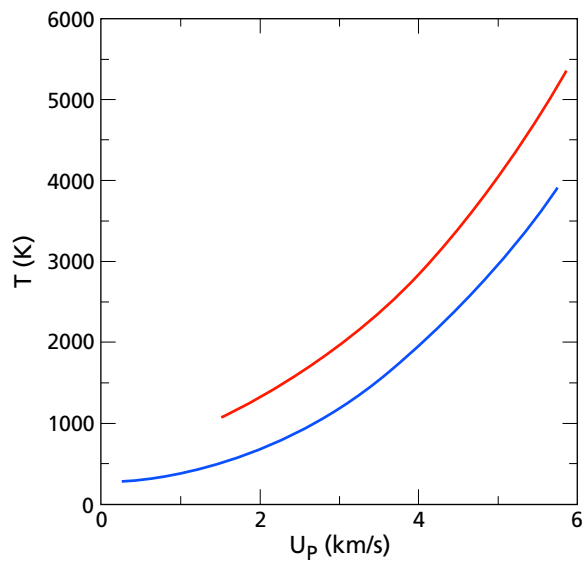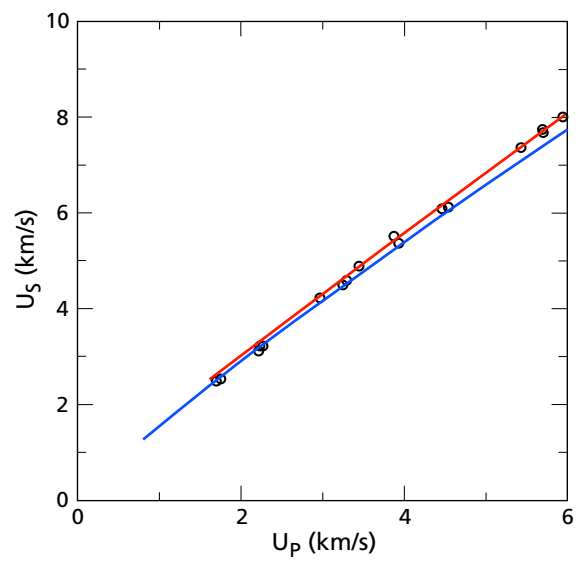
Temperature (K) versus particle (U_P) velocity for Sylgard 184 from the theoretical model: reactants (blue line) and equilibrium products (red line). Note that the reactants temperature is around 1200 K at 3 km/s, high enough that we expect rapid reaction rates.

U_S versus U_P data for S5370 with initial density of 0.496 g/cm³. The equilibrium products EOS theoretical model is given by the red line, and the inert EOS is shown as the blue line. Note that reactant and products Hugoniots are nearly identical. Off-Hugoniot states will vary more between reactants and products due to differences in temperature and composition.

including silicon, mixing with any nearby material containing oxygen (e.g., HE products), can lead to a substantial change in EOS because available silicon will take oxygen away from the normally stable products CO_2 and H_2O.

Validation of the EOS was based on Dynamic Experimentation Division static and shock data on the silicone elastomer Sylgard 184, which is primarily PDMS. The theoretical model is in excellent agreement with the higher particle velocity portion of shock experiments, without any adjustment to match the data. The lower portion of the velocity graph is fit to a cold curve with a reasonable assumption for the Debye temperature, which is related to the distribution of vibrational frequencies. In this case, we choose an effective initial density that is slightly higher than the measured density. This technique takes into account the volume squeezed out at low pressure and gives the characteristic downward curvature of the U_s versus U_p velocity comparison curve at low pressures.

Having demonstrated a good match for the EOS model with a material that is predominately PDMS, the predicted behavior for S5370 should also be very good. The reactants are physical mixtures of

validated component EOSs. The products theoretical model has already been shown to be predictive for closely related compositions. For some cases there is substantial scatter in the experimental data, primarily due to lack of uniform density in the S5370 samples. As anticipated from the evaluation of the Sylgard 184 data, the S5370 equilibrium products EOS is in very good agreement in the region above a particle velocity of 3 km/s where the foam is most likely to be decomposed. Below 3 km/s, the inert EOS is in very good agreement with the data that are expected to be inert. Also, the inert and products EOSs are in a regime where there is very little difference between the two, and both fit the scattered EOS data well. Basically, the difference between the two is smaller than the scatter. Note that the added internal energy per unit mass on the Hugoniot is given by 0.5 U_p^2. Therefore the estimated transition from inert to products is expected to remain ~3 km/s regardless of initial density. It is also important to note that the EOS works well for a wide range of initial densities. That range corresponds to dramatically different temperatures at a given density, implying that the EOS is quite good over a wide region, not just along a line in state space.

A similar process is used for other polymers, such as VCE (ethylene-vinyl acetate-vinyl alcohol terpolymer), where very limited data are available. The theoretical equilibrium products EOS is compared with data on polymers with similar compositions such as the polymer PMMA (Plexiglas, Lucite). When ranges of compositions that essentially span the composition of interest are chosen, the EOS is then validated for accuracy and can be trusted as a good approximation in anticipation of experimental data.

The direction for future work consists of several parallel pieces, each of which is tied to forthcoming experimental data, further evaluation of already available data, and further refinements of the EOS model. In addition to the development of the EOS model, the results must be characterized in a form that can be implemented in hydrodynamics codes. Then the whole model can be compared against intrinsically hydrodynamic data and used to predict the consequences of the effects of shocks on polymer EOSs.

The model for the products EOS will continue to use the thermodynamic perturbation theory approach in the HEOS computer code along with characterization of the solid products. These potentials have already been shown to be in good agreement with a wide variety of data, in particular data not used in the initial characterization. As necessary, they will be further refined as new data become available. Specific choices of materials for future work will follow the schedule of planned experiments unless there is a specific request to start on a polymer or composite sooner. Preliminary products EOSs will be calculated with the current model ahead of experiments. Inert EOSs will follow as data become available on the materials of interest or related materials, as was the case for Sylgard 184 and S5370. Then the model will be validated and/or revised as indicated by the new data as they become available. As the EOSs for new materials are being developed and tested, the SESAME tabular EOS form is being used to produce an EOS that is readily transferred for use in a wide variety of hydrodynamics codes. NWJ

Point of contact:
M. Sam Shaw, 667-5903, mss@lanl.gov

What is an equation of state?

An equation of state (EOS) is a formula describing the interconnection between various thermodynamic properties of a system. Most commonly, the number (and kind) of atoms in the system is fixed (e.g., a mole), or equivalently (except for a factor of the molecular weight) the mass is fixed (e.g., a gram). Probably the best known EOS is that of the ideal gas: $PV = NkT$, where P is pressure, V is the volume, N is the number of particles, k is the Boltzmann constant, and T is temperature. If the independent variables V and T are measured, then P is given by the ideal gas EOS.

We are dealing with a much more complicated system, but the relation between thermodynamic variables can be determined to a good approximation by theoretical methods. For example, given the choice of independent variables V and T for fixed N, the functions $P(V,T)$, $E(V,T)$, $S(V,T)$, and $A(V,T)$ are the pressure, energy, entropy, and Helmholtz free energy in terms of the independent variables. It is easy to show that all of the other thermodynamic variables can be determined from A and its partial derivatives.

Hydrodynamics codes require $P(V,E)$ only. This is sometimes called an incomplete EOS because quantities such as $T(V,E)$ and $S(V,E)$ are not given. Equilibrium theoretical EOSs for explosives and polymers often use the independent variables P and T because the fluid mixture and the solid components must be in pressure and temperature equilibrium. In this case, all of the thermodynamic variables can be determined from $G(P,T)$, the Gibbs free energy, and its derivatives.

High Strain Rate Experiments: Collaborating with VNIIEF

Atlas, the giant US power multiplier or "pulsed-power" machine, has a new home: the Nevada Test Site (NTS).

During the Atlas move, LANL pursued Atlas-like experiments in other venues. One such location was the All Russian Scientific Research Institute of Experimental Physics (VNIIEF) in Sarov, Russia. Coupling existing computer simulation techniques (hydro-codes) like those used to design Atlas experiments and some materials models widely used in the LANL weapons program with a VNIIEF pulsed-power source and Atlas experimental configurations and diagnostics, LANL and Russian scientists collaborated on successful high strain rate (HSR) experiments at VNIIEF in 2003 and 2004. Although Atlas is a multishot facility, VNIIEF has an explosively driven, single-shot, pulsed-power generator that can supply the 35-MA current required for Atlas HSR experiments.

The objective of the 2003–2004 Russian HSR (RHSR) test series at VNIIEF was twofold:

- validate the experimental design, in cylindrical implosion geometry, for later use on Atlas at NTS and

- explore the dynamic strength of a relatively well-studied material (copper) under conditions of high strain applied at very high rate of strain.

During the three-shot RHSR test series (RHSR-0, RHSR-1, and RHSR-2), Russian and LANL scientists evaluated the material strength of copper when it was very rapidly distorted (high strain rate) by measuring perturbation growth at an unstable, copper-fluid interface. Consisting of a low-density "working" fluid (polymer or water) and a copper sample with pre-imposed perturbations of several wavelengths, the interface was accelerated by a magnetically imploded cylindrical liner whose motion pressurized the working fluid. The liner is a shell approximately the size and shape of a tuna can whose motion converts the electrical energy of the generator into hydrodynamic energy to accelerate the interface. For about 10 millionths of a second, the Russian generator—like Atlas—can produce electrical power that is roughly equal to twice the world's total electric power production at any given moment.

Results from each shot in the series were very good. The pulsed-power system delivered 35 MA ±3% in each experiment, reproducing the desired (i.e., Atlas-like) environment with very high precision. A full suite of electrical diagnostics (B-dot, Faraday, and Rogowski loops) performed successfully. At least three independently timed x-ray channels were fielded on each shot; all x-ray sources performed as designed, triggering within 0.1 μs of specified times. Recovery of exposed x-ray film in the high explosive

Russian High-Explosive Pulsed-Power System. The system delivers electrical energy comparable to Atlas but is single use.

(HE) environment is difficult because the HE and shrapnel tend to damage the film holder and protection system; however, excellent collaborative work by the LANL and VNIIEF teams obtained the data needed to meet their objectives.

## Material Strength of Copper

The team evaluated the material strength of a high-grade (M-1) copper sample by comparing the growth of perturbations in time—measured with detailed radiographs during the experiment—with growth predicted by numerical simulation (hydro-code) calculations conducted with relevant strength parameters and several strength models. Periodic perturbations, machined on the surface of the liner, typically are sinusoidal and of different wavelengths (the distance from one sinusoidal crest to the next).

In straightforward evaluations, the team computed (and confirmed analytically) the approximate strain and strain rates the material experienced as the initially small-amplitude, sinusoidal perturbations grew into the "spike and bubble" structure typical of Rayleigh-Taylor behavior.
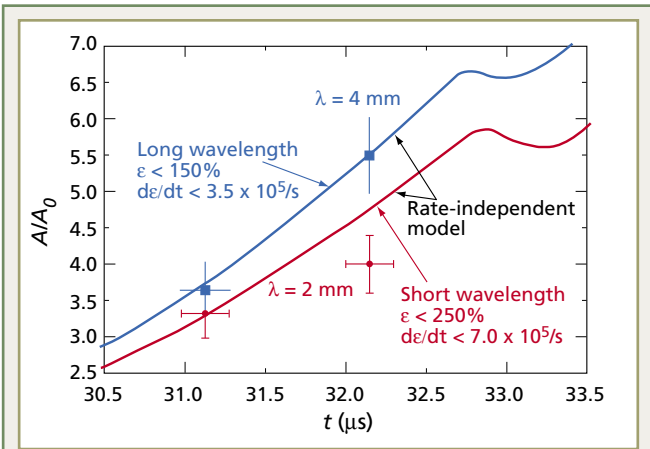

RHSR-2 results with water as the working fluid. A/A_0 is the amplitude of the perturbation compared with the initial amplitude. Solid curve shows the growth of long-(4-mm) and short- (2-mm) wavelength perturbations in M-1 copper predicted by numerical simulation. The data points show results of the RHSR-2 experiment. Agreement is good for 4-mm wavelength but the data show deviations for the 2-mm wavelength; $d\varepsilon/dt$ represents strain rate.
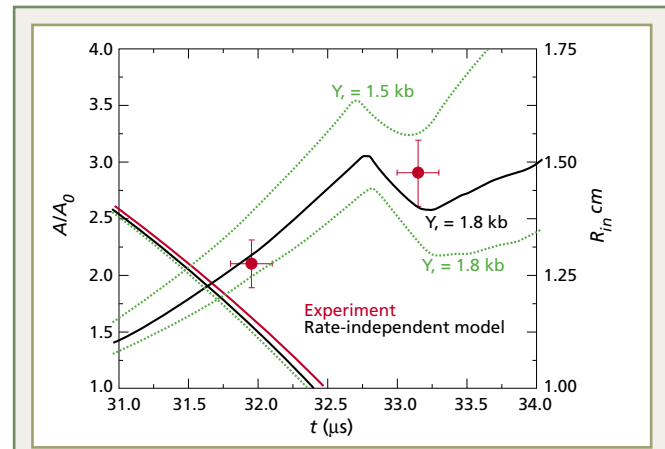
RHSR-1 results with polyethylene as the working fluid. Strength in the polyethylene apparently suppresses perturbation growth. R_{in} shows the implosion trajectory for the inner surface of the copper sample for two calculations (green and black) and for the experimental velocity measurement (red).

Measuring perturbation growth. A magnetically driven liner (yellow) compresses and accelerates a working fluid (blue). In RHSR experiments the fluid was either polyethylene or water. The growth of long- and short-wavelength perturbations, measured radiographically, is evaluated against the growth of perturbations predicted for various strength models. "Synthetic radiograph" shows results from the numerical simulation displayed as a radiograph for visual comparison with the experimental data ("Experimental radiograph").
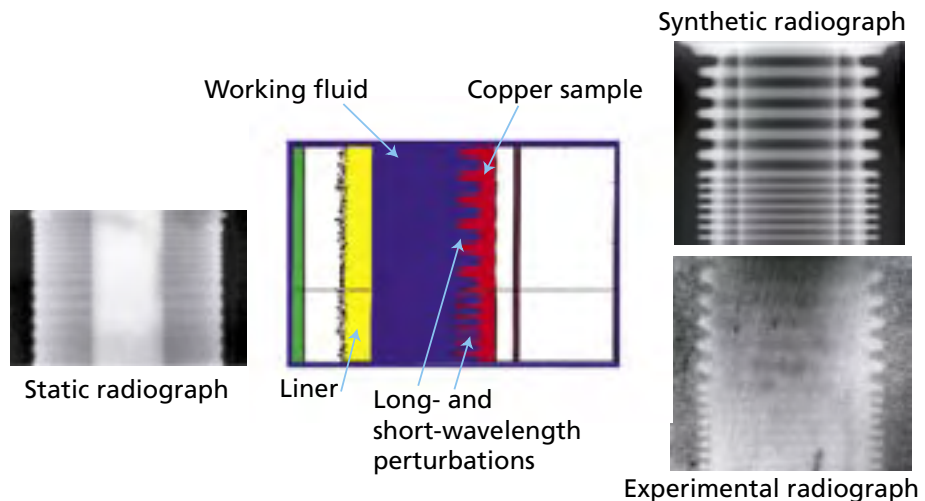
In the RHSR series under acceleration conditions, the peak strain for perturbations with a wavelength of 4 mm was approximately 150%; peak strain rate in the materials was approximately 3×10^5/s. For the smaller, nominally faster-growing 2-mm wavelength perturbations, the maximum strain was approximately 250% and the peak strain rate was approximately 7×10^5/s.

Using rate-independent strength models such as Glushak (in Russia) or Steinberg-Guinen (in the US), the team accurately predicted the growth of the relatively long (4-mm) wavelength perturbations. Their findings suggest that a rate-independent model of materials strength may adequately describe material behavior for conditions involving strain up to approximately 150% and strain rates up to 3×10^5/s.

However, hydrocode results, again calculated with strain rate-independent models, did not show similarly good agreement with short-wavelength (2-mm) data from the same experiment. This disagreement suggests—but does not prove—that at higher strain rates, some additional physical insight (probably rate dependency) is needed to adequately describe the behavior of the material for strain rates of 7×10^5/s and higher.

Strength of Polymer Materials

Two of the copper experiments were conducted using a polymer (polyethylene) working fluid and one was conducted using water as the working fluid. Water has virtually no strength and the static strength of the polyethylene is only a few tens of bars. These characteristics suggest that the same results should be obtained with either working fluid. Surprisingly, perturbation growth in the copper sample was dramatically lower in experiments that used a polyethylene working fluid than in experiments that used water as a working fluid. Using a 1-parameter (yield strength) von Mises-based model, the team evaluated the apparently increased strength displayed by the polyethylene at strains and rates accessed in this experiment compared with polyethylene's static properties. The team's assessment that the polyethylene displayed yield strength 16 to 20 times that of the polyethylene under static conditions—an apparent yield strength of 1 to 2 kb—may be the first direct, quantitative evaluation of polymer strength at these strains and rates.

VNIIEF Experiments

In related VNIIEF experiments using direct HE-driven, planar (flat) rather than cylindrical (tuna-can-shaped) geometry, results similar to those observed during the RHSR tests were also obtained.

In the planar experiments, while perturbation growth was in good agreement with the rate-independent predictions for longer wavelengths, the team noted substantial differences between experimental data and numerical simulations at shorter wavelengths (a characteristic of higher strain rates). However, in the planar data, growth rate at short wavelengths was faster than the growth rate predicted by the hydrocodes. In the cylindrical data, growth rates were smaller than predicted by rate-independent models.

Comparing planar and cylindrical results, the VNIIEF–Los Alamos team made the following observations:

• planar experiments are the best way to collect an extended data set to evaluate dynamic strength effects in copper;

• Atlas experiments in cylindrical geometry can reach higher strain rates than can be achieved in direct HE-driven planar experiments by applying no-shock, magnetic pressure loading for a longer period of time; and

• by decreasing both perturbation wavelength and the radius-wavelength ratio, it is reasonable to expect that the effects of curvature leading to 2-D strain fields present in cylindrical geometry will become more pronounced.

The team then concluded that both planar and cylindrical experiments are needed to fully explain strength effects at high rates of strain.

Benefits of RHSR Series

The RHSR test series effectively accelerated the Atlas experimental program by conducting experiments originally scheduled at NTS after Atlas was recommissioned. The RHSR series (1) demonstrated successful performance of the liner-driven, cylindrical perturbation-growth technique and (2) produced what may be the first recorded quantitative data using this technique with metals in cylindrical geometry.

As a result of the RHSR data, the Atlas-HSR experiment series will be modified to take better advantage of Atlas' unique features, such as higher strains and strain rates and higher precision in control of energy delivery to the experiment, and to emphasize Atlas' capability to explore multidimensional strain fields at high strain rates.

Perhaps the greater though less-tangible benefit of joint LANL-VNIIEF experiments lies in their continuing potential to foster Russian-US scientific collaboration that advances the nonproliferation goals of both nations. **NW**

Points of contact:
Walter Atchison, 665-3984, wla@lanl.gov
Robert Reinovsky, 667-8214, bobr@lanl.gov

RHSR Team

An interdisciplinary, interdivisional team planned and executed the RHSR experiments. Anatoli Buyko, Vladislav Mokhov, Alexander Petrukhin, and Andrey Ivanovsky led the 50-member Russian experimental/theoretical team.

LANL's team included Walter Atchison and Ann Kaul (X-1); David Oro, Russell Olsen, John Stokes, Brodie Anderson, Leonard Tabaka, Darin Wesley, and Adam Montoya (P-22); George Rodriguez and Quinn McCullough (MST-10); Pat Reardon, Mike Salazar, and Jeff Griego (MST-7); and Jim Goforth and Hank Oona (DX-2).

Russian-LANL RHSR experimental team during the RHSR-2 experiment in February 2004. US and Russian scientists collaborated on Atlas-type experiments at VNIIEF in 2003 and 2004.

Theory and Simulation of the Aging of PBX 9501

The plastic-bonded high explosive PBX 9501, used extensively in weapons, is 94.9% by weight HMX explosive, 2.5% Estane® 5703, 2.5% nitroplasticizer, and 0.1% Irganox 1010 stabilizer (antioxidant). Noveon's Estane® 5703 is a commercial thermoplastic that serves as glue that binds the HMX crystals together to allow the machining of high-precision PBX 9501 parts.

Polymers consist of small molecular units, called monomers, that form chemical bonds to other monomers to make up very large molecular chains (macromolecules). A copolymer is a polymer derived from the linking of two or more different kinds of monomers. Estane, a poly(ester urethane), is a copolymer made up of urethane and ester monomers randomly linked. The nitroplasticizer softens the Estane and improves the processing characteristics; together they markedly decrease the mechanical sensitivity of the PBX. However, the Estane slowly degrades over time, and the corresponding effect on the mechanical properties of the PBX raises safety and reliability concerns. Hence, the study of polymer aging is an integral part of the Enhanced Surveillance Campaign.

These aging studies are being carried out by experimentalists here at LANL and at the Pantex Plant at Amarillo, Texas. We are studying the chemical
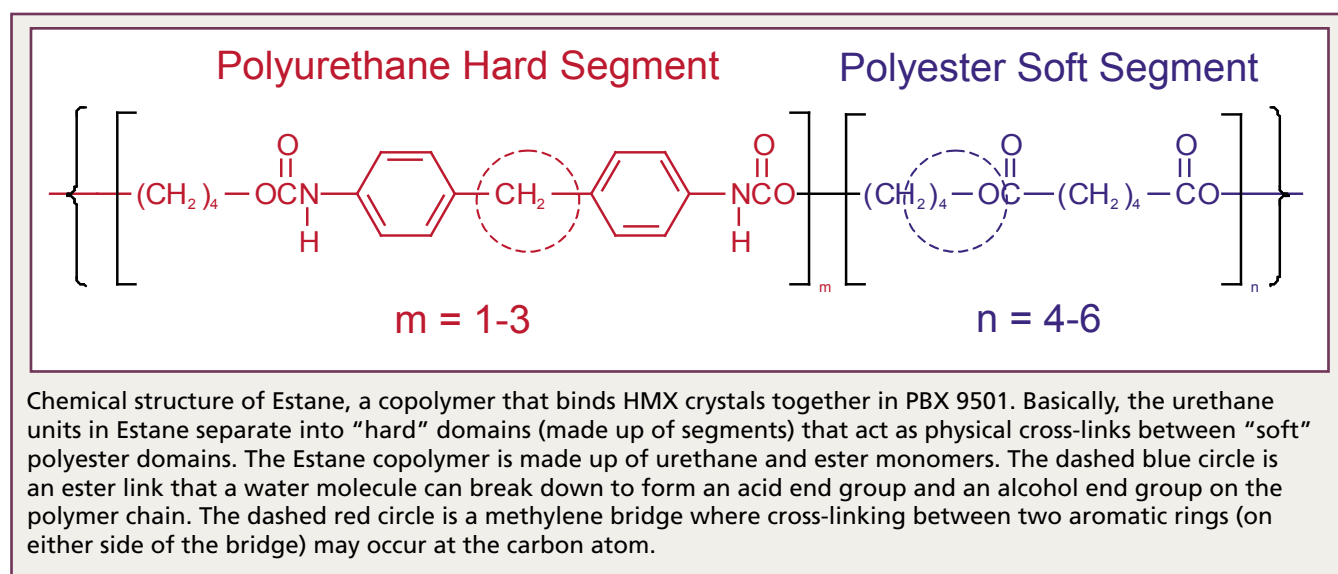

Estane slowly degrades over time, and the corresponding effect on PBX 9501 raises weapon safety and reliability concerns.

---

mechanisms of degradation processes in PBX 9501 and are developing kinetics models. We are working to determine the chemical and mechanical properties of PBX 9501 and how the two are related. Our goals are to understand the chemical mechanisms by which the components of PBX 9501 age and to develop models that reliably predict the chemical composition and molecular weight of Estane for periods of time longer than the ages of any of the weapons.
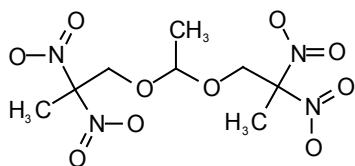
The structure (morphology) of Estane is complicated. The urethane monomers consist of m = 1 to 3 repeat units, and the ester monomers consist
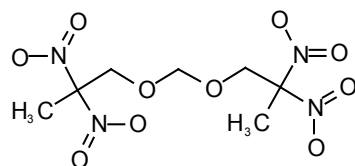

Chemical structure of Estane, a copolymer that binds HMX crystals together in PBX 9501. Basically, the urethane units in Estane separate into "hard" domains (made up of segments) that act as physical cross-links between "soft" polyester domains. The Estane copolymer is made up of urethane and ester monomers. The dashed blue circle is an ester link that a water molecule can break down to form an acid end group and an alcohol end group on the polymer chain. The dashed red circle is a methylene bridge where cross-linking between two aromatic rings (on either side of the bridge) may occur at the carbon atom.

of n = 4 to 6 repeat units. Urethane units tend to clump together (phase separate) into "hard" domains that act as physical cross-links, giving the polymer its strength, between the "soft" polyester domains that provide flexibility. The domains are made up of collections of segments. Not all hard segments participate in hard domains; on the average, there has to be a critical number of segments before a polymer chain participates in a hard domain. Poly(ester urethanes), such as Estane, are known to be degraded by thermolysis (heat), photolysis (light), hydrolysis (water), and oxidation (air pollutant gases).

Until now, this cooperative theory and simulation task has been focused on the hydrolysis of the ester links in the soft domains. Estane has been shown to hydrolyze via an acid-catalyzed mechanism in which a water molecule attacks an ester link and forms an acid end group and an alcohol end group on the polymer chain. The breaking of the ester links leads to a decrease in molecular weight (MW) of Estane that is exposed to the atmosphere at ambient humidity. A single set of rate coefficients for this mechanism was obtained by fitting to several different hydrolysis experiments (measured change in MW versus time) conducted at LANL, Pantex, the Kansas City Plant, and Sandia National Laboratories. These rate coefficients are now being employed in a kinetics model of PBX 9501 hydrolysis to simulate the change in MW with time observed in natural and accelerated aging.

Recently we embarked on a new study of another degradation mechanism, the free-radical oxidation of the urethane segments, to determine which mechanism dominates in weapons storage. Free-radical oxidation may be as important as hydrolysis, especially as the PBX dries out, because the storage environment has both low moisture and low oxygen content. The nitroplasticizer is composed of a mixture of two molecules, bis-2,2-dinitropropyl acetal (BDNPA) and bis-2,2-dinitropropyl formal (BDNPF). The mixture usually used is 45% BDNPA and 55% BDNPF by weight because this particular mixture, a liquid at room temperature, can plasticize (soften) polymers.

Research efforts show that upon heating, the nitroplasticizer loses nitro (NO_2) groups and produces oxidizing species that can degrade Estane. The experimental evidence includes the following (from experiments all carried out at LANL):

(1) identification of stable radicals by electron spin resonance (ESR) after exposing 50/50 mixtures of nitroplasticizer/Estane to x-rays and oxygen;

Container used in the CAS and jar with Estane pellets. Over 1,000 of these containers containing samples, made up of 25 different combinations of constituents of PBX 9501, were placed in ovens and held at a fixed temperature for specified intervals of time. Decomposition gases were extracted from each container and the chemical makeup determined.

Chemical structures of the two nitroplasticizer molecules BDNPA and BDNPF. The nitroplasticizer, composed of a mixture of these two molecules, is used to soften polymers.

Bis-2,2-dinitropropyl acetal (BDNPA)

Bis-2,2-dinitropropyl formal (BDNPF)

(2) identification of the oxidation of the methylene bridge in the urethane unit via ^{13}C nuclear magnetic resonance (NMR) spectroscopy;

(3) observation of small changes in the NO_2 region of the ^{15}N NMR spectrum after reacting isotopically labeled nitroplasticizer with labeled Estane or an Estane analog; and

(4) loss of infrared (IR) transmission intensity in the NO_2 region after heating nitroplasticizer in a diamond anvil cell.

The Constituent Aging Study (CAS) being conducted at Pantex is producing exciting results on the oxidative degradation of Estane. The CAS goals are to artificially age the PBX 9501 constituents (HMX, Estane, nitroplasticizer, stabilizer) in 25 different combinations at accelerated rates, detect chemical reactions that take place, identify reaction products and possible degradation mechanisms, and provide data for lifetime prediction modeling.

The samples are aged at different temperatures (ranging from 40°C to 64°C) in a dry, oxygen-free environment. Over 1,000 samples were aged for a period of 3 years, with typical samples analyzed at half-year intervals. Reaction rates are measured for the aged samples to establish the temperature dependence (Arrhenius equation) for the rates:

$$A \exp(-E_a/RT),$$
where
    A is the prefactor,
    E_a is the activation energy,
    R is the gas constant, and
    T is the temperature.

Based on the rate of evolution of NO_x (N_2O and NO) gases at various temperatures, the Arrhenius parameters A and E_a for nitroplasticizer decomposition rates were determined for eight different CAS constituent combinations. The eight sets of Arrhenius parameters are plotted as ln(A) versus E_a (note the narrow range in E_a). The well-known kinetic compensation effect is demonstrated—small changes in ln(A) are compensated by small changes in E_a in a linear relationship. One of the most striking findings is that combinations containing nitro-

plasticizer (nitroplasticizer + Estane, nitroplasticizer + Estane + stabilizer) show a strong correlation between the total amount of gas products generated and significant changes in the Estane MW.

A likely mechanism for these changes is that NO_2 groups dissociate from the nitroplasticizer molecules and subsequently oxidize the carbon atoms in the backbone of the nitroplasticizer molecules as well as oxidize the urethane linkages in Estane. The oxidation of the Estane polymer can cause chain scission (decreased MW) and cross-linking (increased MW and gel formation), while small molecule remnants of the reactions are presumably detected in the gas analysis. Such large changes in MW can have drastic effects on the mechanical properties of the elastomer. The energy of activation (E_a = 28 kcal/mol)
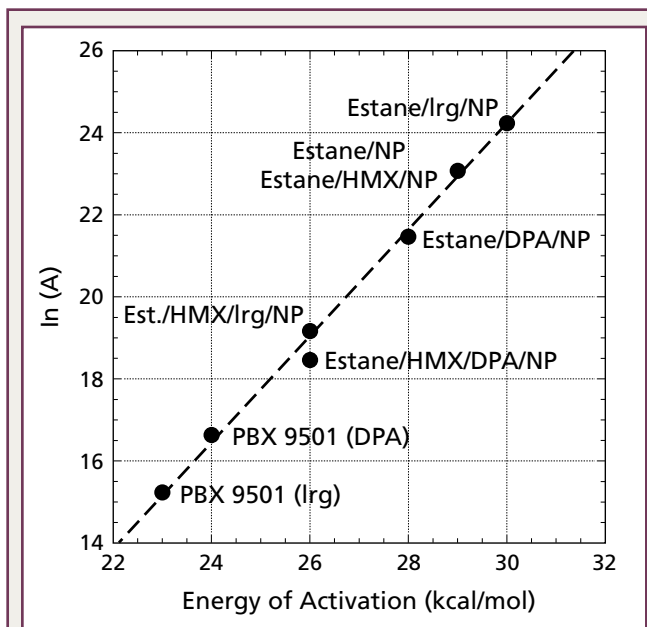
Arrhenius parameters for the rate of NO_x gas evolution from eight different CAS combinations (out of a total of 25 combinations) of PBX 9501 constituents. The prefactor A is in units of per second. The kinetic compensation effect, small changes in ln (A) compensated by small changes in E_a in a linear relationship, indicates that all eight combinations are capturing the same chemical rate process, presumably that of nitroplasticizer decomposition. For each combination, the constituents are labeled: Est. = Estane, Irg = Irganox 1010 (stabilizer), NP = nitroplasticizer, DPA = diphenylamine (stabilizer). The combinations labeled PBX 9501 are made up of Estane, HMX, nitroplasticizer, and stabilizer—either Irganox (Irg) or DPA—formulated in the same weight ratios as the actual explosive.

for the rate of evolution of NO_x gases compares favorably with values determined by an earlier aging study on PBX 9501. Finally, preliminary CAS findings suggest that the stabilizers (DPA and Irganox 1010) may not be optimum because the antioxidant is intended to prevent—not enhance—cross-linking, one of the free-radical degradation reactions.

The overall goal in the modeling and simulation effort is to construct a detailed chemical kinetics mechanism that describes the oxidation of Estane in the presence of nitroplasticizer that is consistent with the data provided by the CAS and other experiments. Questions that need answers include the following:

- Where along the Estane hard segment are the chemical changes taking place, and what are the chemical identities of the reactants? Both the location of the chain scissioning and the location and chemical identity of structures of the cross-links need to be determined.

- Does scissioning take place as depolymerization (forming isocyanate and alcohol) by breaking the bond between the oxygen and carbon atoms on the backbone of the polymer chain?

- Does cross-linking occur at the carbon atom on the methylene bridge between the two aromatic rings (as suggested by ^{13}C NMR studies and identification of the aldehyde oxidation product)? At the nitrogen atom on the amide group (as suggested by IR spectroscopy studies of the products of the oxidation of urethane by atmospheric molecular oxygen)? At a carbon atom on the aromatic ring?

- Do the cross-links consist of direct bonds between the two polymer chains? Fragments from the nitroplasticizer molecules? Fragments from the stabilizer molecules?

In ongoing work, NMR analysis of the gel (cross-linking) formed from isotopically labeled nitroplasticizer, Estane model compounds, and/or stabilizer could provide some clues to the identity of the cross-linker. We will continue our experiments designed to identify explicit chemical reactions in the mechanism and determine rate constants necessary to perform numerical simulations of the kinetics of nitroplasticizer decomposition and subsequent free-radical oxidation of Estane. [NW]
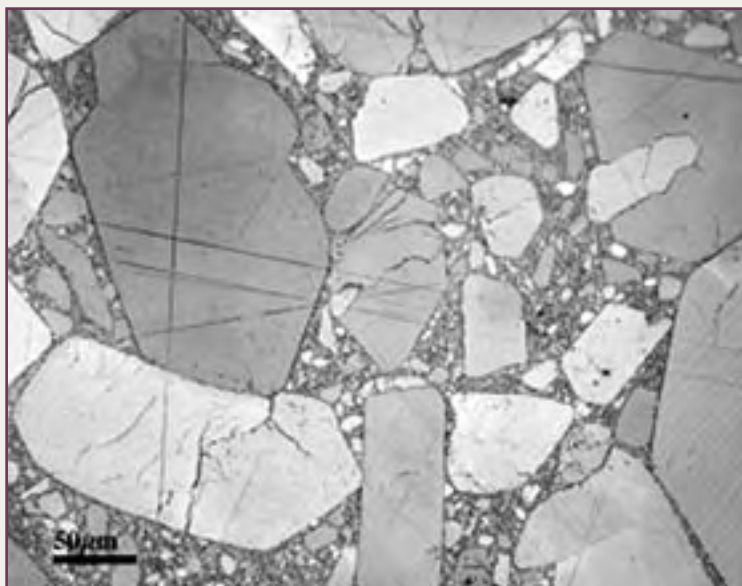
Polarized light microscopy image of a pressed piece of the HE PBX 9501, showing significant cracking and fracturing of the HMX crystals that occurred during pressing. The darker regions between the larger crystals in the image are composed of fine particles of HMX and binder. The binder consists of 50% Estane 5703 poly(ester urethane) polymer and 50% nitroplasticizer.

Total Scattering: The Key to the True Atomic Structure of Complex Materials

The only neutron scattering instrument in the world that is dedicated to total scattering measurements of disordered crystalline materials, ranging from high-temperature superconductors to zeolites, is the Neutron Powder Diffractometer (NPDF) at LANL.

The NPDF has operated at the Manuel Lujan Jr. Neutron Scattering Center at the Los Alamos Neutron Science Center (LANSCE) since September 2002. The Lujan Center, at the end of the beamline from the LANSCE proton accelerator, is a pulsed spallation neutron source equipped with time-of-flight spectrometers for neutron scattering studies of condensed matter. The Lujan Center provides 16 neutron flight paths for thermal and cold neutron experiments.
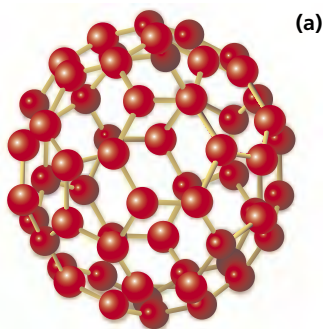

The NPDF is located at flight path 1 at the Lujan Neutron Scattering Center. The instrument was recently upgraded for a total cost of $1.1M shared by the National Science Foundation, several academic institutions, and LANL. The NPDF is now among the world's leading diffractometers, specialized in the study of the atomic structure of complex materials.

Knowing the atomic structure of a modern, complex material is the key to a deeper understanding of its properties. The goal is to link macroscopic properties to the atomic structure to ultimately be able to predict material response and manufacture materials with a set of desired properties—for example, matching the shock response of stockpile materials to legacy materials made by obsolete processes.

Total scattering is a method used to obtain structural information. Traditional structure determination from a scattering experiment is based on analysis of the intensity and position of Bragg reflections. This technique, applied to single-crystal or powder-diffraction data, is now routine and has contributed significantly to our knowledge of materials for approximately 50 years. However, one should remember that the atomic structure determined by these measurements is an average long-range structure. The diffraction pattern, on the other hand, contains not only Bragg intensities, but also additional diffuse scattering that contains information about deviations from this average structure in the form of defects. The sum of Bragg reflections and diffuse scattering is referred to as total scattering, which reveals the true local, medium, and long-range atomic structures of the material.

Atomic Pair Distribution Function

One convenient way to study total scattering of polycrystalline or glassy materials is the pair distribution function (PDF) analysis. This technique has its origins in the study of glasses and liquids but can be applied in a similar fashion to disordered crystalline materials ranging from simple alloys exhibiting chemical short-range order to the complex local structure found in materials such as high-temperature superconducting oxides.

The PDF, $G(r)$, is simply obtained via Fourier transform from properly normalized scattering intensities, and it gives the probability of finding two atoms at a specific distance, r. This probability allows one to study the atomic structure of a given material as a function of length scale within the structure.

For example, consider solid C_{60} as a microstructured material made up of C_{60} buckyballs. The diameter of each C_{60} molecule is approximately 7.1 Å. Sharp pe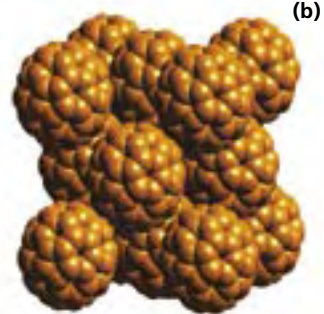aks are observed in the PDF coming from the characteristic carbon-carbon pairs on the ball up to the molecular diameter of 7.1 Å. Thereafter, only a broad, featureless structure exists. The sharp peaks are the intramolecular structure and the broad peaks feature the intermolecular structure, or ball-ball correlations.

The goal is to predict material response and manufacture materials with a set of desired properties.

The PDF provides the local, medium, and long-range atomic structure in a single experiment. At total scattering, the experiment requires a large range in momentum transfer space as well as a low intrinsic background signal. Suitable experimental conditions can be found at synchrotron sources using high-energy x-rays or spallation neutron sources such as LANSCE. The advantage of using neutrons instead of x-rays is their sensitivity to light elements such as hydrogen, the constant scattering power as a function of scattering angle due to a lack of an atomic form factor, and their high penetration power. The latter is particularly useful if the experimental sample being studied requires significant containment. The downside of using neutrons is that large sample amounts are required and measuring times are typically longer compared with x-ray measurements.

NPDF Instrument

The unique feature of the NPDF is its high resolution applied to the PDF technique. High resolution in momentum space translates to a large range in r-space (distance) in the resulting PDF of up to 200 Å or 20 nm, illustrated by a measurement comparing gold nanoparticles with bulk gold. The transmission micrograph shows that the average size of the gold nanoparticles is 36 Å or 3.6 nm.

In many ways scientists have just started to exploit the full potential of PDF measurements over various ranges of atom-atom distances, but it is clear that in many cases the atomic structure obtained by conventional structure determination methods is insufficient to structurally characterize materials. The PDF method allows one to extract a true structural picture over a variable range, giving

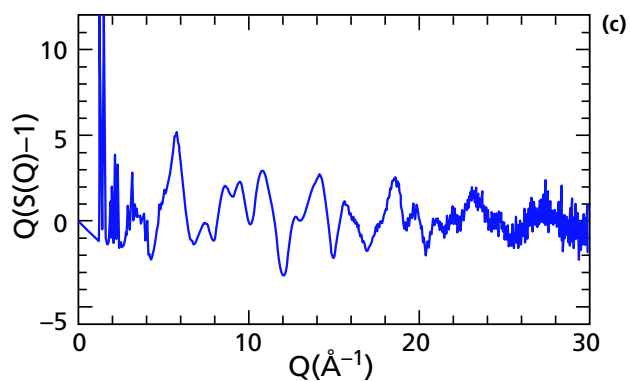So-called buckyballs or C_{60} molecules (a) can be assembled into long-range ordered crystals (b). The normalized neutron scattering intensities (c) are Fourier transformed to obtain the PDF (d). Note that the PDF shows sharp peaks for distances (r) smaller than the diameter of a single C_{60} molecule, indicated by the vertical dashed line. These peaks correspond to the carbon-carbon atomic distances within a single molecule. For larger distances no such peaks can be observed, indicating that, in this measurement taken at room temperature, no correlations exist between carbon atoms from different C_{60} molecules.
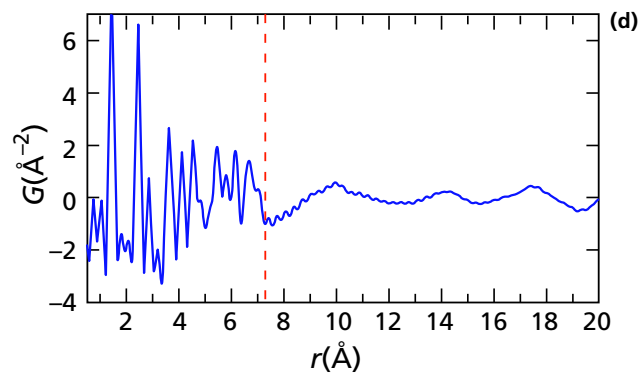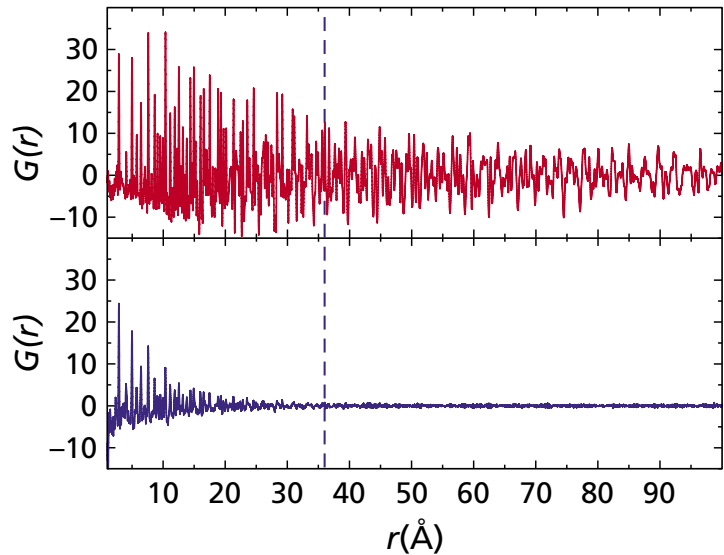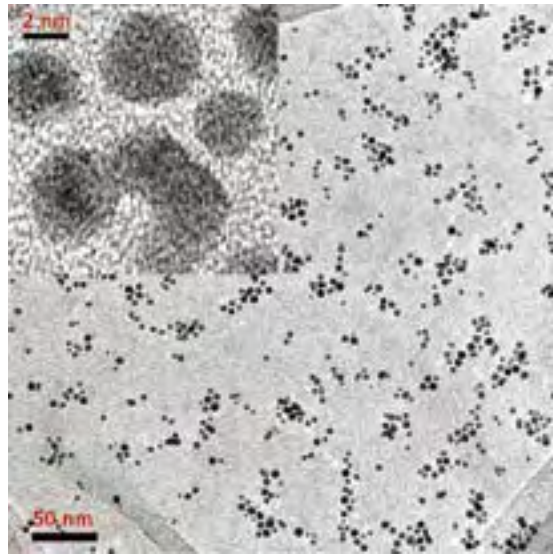
(a)

(b)

(c)

(d)

A transmission electron micrograph of gold nanoparticles is shown on the left. The average particle size is 36 Å. The graphs on the right show the PDF of bulk gold (top) as well as that of the gold nanoparticles (bottom). Note that the PDFs show gold-gold atomic distances out to an unprecedented distance of 100 Å, now possible on the upgraded NPDF instrument. The vertical line marks the average particle size, and it is obvious that atom-atom correlations larger than this distance exist in the bulk material but not in the nanomaterial as one would expect.

much deeper insight into the structure-property relationship of materials, which is the central question in all material science, but is more specifically the central question for materials in the nuclear weapons stockpile. NWJ

Point of contact:
Thomas Proffen, 665-6573, tproffen@lanl.gov

DEFINITIONS

medium-range structure—The range between local structure and long-range structure.

momentum transfer space—The momentum transfer Q is defined as $Q = 4\pi\sin(\theta)/\lambda$, where θ is the scattering angle and λ is the wavelength of the neutron or x-rays used. Obviously, short wavelength or high-energy radiation is desired to obtain large values in Q.

local structure—The atomic structure over a range of a few nearest neighbor atoms.

long-range structure—The averaged periodic structure of a crystalline material.
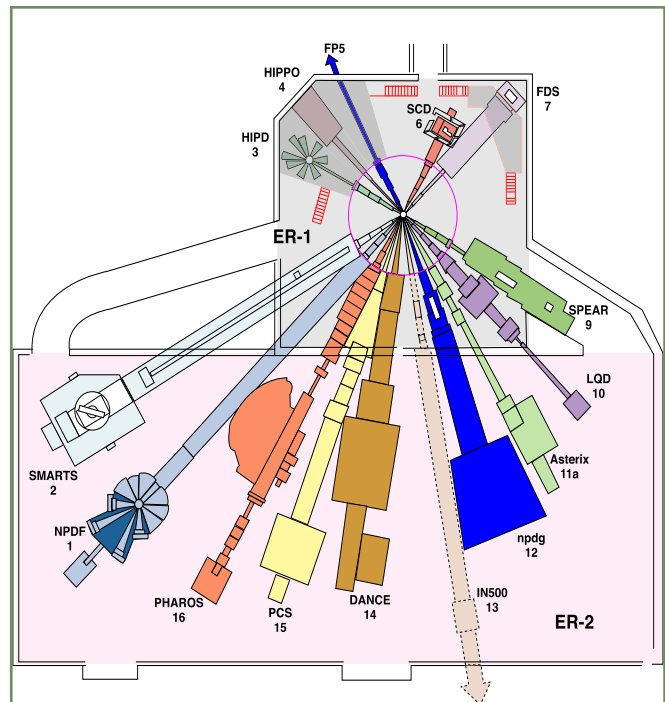
The Lujan Center's instrument suite. The tungsten spallation target (cylindrical feature in ER-1) accepts proton beam from the Proton Storage Ring aimed vertically down by steering magnets. The instruments view moderated neutrons through 16 penetrations in the bulk shield.

The Human Reliability Program— Mitigating the Insider Threat

One of the DOE's overriding national security priorities is ensuring the integrity and safety of the country's nuclear weapons. The DOE has implemented the Human Reliability Program (HRP) to ensure that individuals who hold HRP-designated positions meet the highest standards of reliability, including physical and mental stability, in support of national security.

In July 2004, the Laboratory adopted the requirement of 10 CFR 712, the HRP, to combine the Personnel Assurance Program, a nuclear safety program, and the Personnel Security Assurance Program, a nuclear security program, into the HRP.

The HRP, administered by the Laboratory's Personnel Security Group, targets the Q-cleared individual whose job

- allows access to Category I levels of special nuclear material (SNM) or includes the responsibility for transportation or protection of Category I quantities of SNM;

- involves nuclear explosive duties, i.e., hands-on work with, or access to, nuclear explosives or responsibility for working with, protecting, or transporting nuclear devices or selected components;

- permits access to information concerning vulnerabilities in protective systems when transporting nuclear explosives, nuclear devices, selected components, or Category I quantities of SNM; or

- is not included in the above but has the potential to significantly impact or cause unacceptable damage to national security.

Line management and program administrators determine which employees are in the HRP. Employees who participate in the HRP must

- complete the Questionnaire for National Security Positions, Part 2, annually;

- receive a physical examination and a psychological evaluation annually;

- receive a psychological evaluation initially, and subsequently every third year, that includes at least one objective psychological testing instrument;

- take initial and then random, unannounced urine drug and breath alcohol tests at least once within a 12-month period;

- complete initial and annual HRP training and required security refresher training; and

- complete a counterintelligence-scope polygraph test.

Individuals who hold HRP-designated positions meet the highest standards of reliability in support of national security.

Some personal privacy is sacrificed implementing the HRP. In fact, the program is a good example of the pivotal point at which national security needs exceed the individual's right to privacy as guaranteed by the Fourth Amendment to the Constitution. The Supreme Court ruled in 1989 that safety and security concerns may override Fourth Amendment rights. The Laboratory has made every effort to negotiate with the DOE to keep the sacrifice of personal privacy to a minimum. Recorded details such as drug/alcohol test results, medical assessments, and reports of security concerns are maintained in the strictest confidence.

Standards of judgment and reliability for weapons program employees are determined by a continuous

evaluation to identify individuals who may be impaired by physical or mental/personality disorders, alcohol abuse, use of illegal drugs, abuse of legal drugs or other substances, or any condition or circumstance that may be a safety or security concern.

The continuous evaluation is formalized every year, and the individual is certified in writing by the immediate supervisor, the site occupational medical director after the physical/psychological examination, the HRP manager, and DOE/NNSA Office of Personnel Security. The DOE/NNSA HRP certifying official assesses any security concerns or the absence of security concerns that may have arisen in the evaluation processes and decides whether to grant/continue or to deny/revoke an individual's HRP access authorization.

HRP employee reporting responsibilities are the same for any L- or Q-cleared individual, including

- all arrests and criminal charges, in addition to those that were dismissed, detentions by a law enforcement authority, or traffic violations with a fine of $250 or greater;

- bankruptcy;

- garnishment of wages;

- legal action initiated for a name change;

- change of citizenship;

- employment by, representation of, or other business-related association with a foreign or foreign-owned interest or foreign national; and

- marriage or cohabitation.

In addition to those security issues, HRP employees must report any

- physical or mental condition that may require medication or treatment;

- sick leave of 5 or more consecutive working days; and

- medication that may impact a person's physical or mental capabilities, e.g., labels that state "do not drive or operate machinery" or "may cause drowsiness." If an employee believes that a medication could impact his/her reliability or judgment, the employee must report the medication to the Laboratory's Occupational Medicine Group.

A few prescription drugs and some over-the-counter drugs and food products may result in positive findings in the screening and/or confirmation tests. Employees should feel secure that positive results from such products are protected from being a "verified illegal positive" by the quality assurance steps of the testing laboratory, the medical review officer's compliance with protocol, and specialized compound assays when necessary.

Employees are advised not to stop taking a prescribed drug or effective over-the-counter medication if they fear a positive finding on a drug test. If medication causes a positive drug test result, the employee will meet with the medical review officer, who will call the employee's pharmacist or physician for verification and attach a copy of the prescription to the employee's medical file to mitigate the positive finding. In these cases, the medical review officer will report the drug test result to the HRP as a negative.

The employee, the employee's supervisor, a division-level manager, or the site occupational medical director or designee may request temporary removal of the employee from an HRP position. Temporary removal may result from identification of a potential security concern or from identification of a condition, such as illness, that may temporarily affect the employee's ability to perform his or her normal work. Temporary restrictions for nonsecurity concerns may be reinstated locally, i.e., at the Laboratory. If the temporary removal results from a security concern, only the DOE HRP certifying official can approve reinstatement. NWJ

Point of contact:
Eric D. Dick, 667-6018, edick@lanl.gov

RACER:
Transparent Environmental Data

Risk Assessment Corporation (RAC), a small team of independent environmental consultants, is conducting a project that not only will change the way LANL makes environmental-risk-reduction decisions, but also will present—in a user-friendly context—LANL's methods of validating and verifying the data used to make such decisions.

Because the data indicate the concentrations and kinds of contaminants Laboratory operations have released to the environment, the Laboratory uses these data to prioritize and plan environmental cleanup and remedial actions.

Although LANL and other groups have collected data concerning the Laboratory's impact on the environment, the data resided in numerous locations and were difficult for the public to access and/or put into perspective. Now, however, the Risk Analysis, Communication, Evaluation, and Reduction (RACER) Project is creating one public-friendly database that in time will house all LANL-related environmental data.

RACER has three objectives:

1. develop a transparent process for identifying, quantifying, and managing public health risks and ecological impacts associated with chemicals and radionuclides released into the environment as a result of LANL operations;

2. create a database of all pertinent LANL environmental data in a publicly available web site that has robust query tools; and

3. establish a defensible process, based on a risk calculation tool, that LANL can use as a guide to continuous and demonstrable risk reduction.

Key Elements

Risk-ranking methodologies, particularly those the Laboratory uses to evaluate its options for curtailing public health risk, must be sufficiently flexible to accommodate inevitable changes in technology and public values. Incorporating that criterion, RACER has two key elements: a risk-calculation tool and a decision-support tool. Both will be web-based and both will help quantify the factors used to identify and set priorities for environmental risk reduction.

RACER's goal is a transparent risk-analysis process.

The risk-calculation tool will provide a relative ranking of health risks and ecological impacts associated with chemicals and radionuclides released into the environment as a result of LANL operations. It will emphasize prioritizing sources of risk and clarifying the overall risk of different potential remedial options.

The decision-support tool will ensure that many important factors are considered before the Laboratory makes final recommendations for environment-related, risk-reduction decisions. Because such decisions should not be based solely on level of risk, determinants such as cost, available technology, and potential ecological and cultural impacts must be factored into the decision-making process.

In addition, to establish appropriate comparative criteria for risk-reduction options, LANL must directly involve the organizations and individuals affected by or interested in the risk-analysis process. Therefore, the decision-support tool also will incorporate decision criteria that reflect stakeholder input. Stake-

holders are individuals or organizations who have a personal, financial, health, or legal interest in activities, policy, or recommendations that affect their well-being or their environment—i.e., any person or party who has an interest in or is affected by LANL's ecological and environmental risk-reduction methodologies.

RACER's objective is a straightforward risk-analysis process that incorporates the concerns of a variety of stakeholders; to achieve this transparency, a steering panel will identify stakeholder issues. The steering panel will include representatives from the Los Alamos business community, county council, nearby pueblos, the US Department of Energy, and other interested groups.

Availability

Although the purpose of the RACER database is to provide a single access source for all LANL-related environmental data, some aspects of the RACER Project are already in place. For example, a significant percentage of these data now can be accessed from one uniform database, which is available for comment at http://www.racteam.com/LANLRisk/RACERDatabase.htm. An early RACER Project milestone, the database is structured to accommodate data from LANL and New Mexico Environment Department (NMED) data-collecting groups, as well as the US Geological Survey, Environmental Protection Agency, local citizens' groups, Pueblos, and other organizations that collect environment-related data associated with LANL activities.

Containing thousands of entries, RACER allows users to compare its data in several ways: spatially, temporally, across data-collecting organizations, and with applicable standards or background levels.

RACER's developers believe that public accessibility and a user-friendly system will increase public understanding of how LANL operations—both past and present—impact local and surrounding environments. A fundamental principle guiding the developers is that all LANL-related environmental monitoring data should be publicly available, easily accessible, and presented so that anyone can understand how the data were gathered and how they are used to determine environmental risk-reduction activities. Although the database is still in development, several non-LANL groups have already applauded its ease of use.
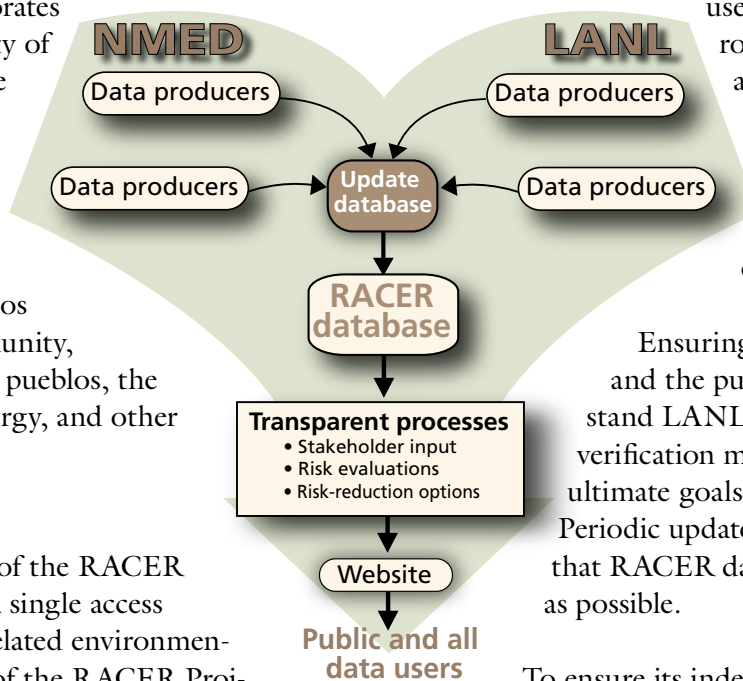
Ensuring the data's credibility and the public's ability to understand LANL's data validation and verification methodologies are the ultimate goals of the RACER Project. Periodic updates are planned to ensure that RACER data are as comprehensive as possible.

To ensure its independence from the Laboratory, RACER is funded by LANL through Colorado State University. To further ensure its independence—and credibility—RACER eventually will be housed at a non-LANL public institution (yet to be selected) that is physically removed from the Laboratory. All data will be accessible to the public through a website that will summarize the verification and validation techniques used by each LANL and NMED data-collecting group. NWJ

Points of contact:
John Till, 665-8886, jtill@racteam.com
Jill Aanenson, 665-8886, jaanenson@racteam.com

NMED — Data producers, Data producers → **Update database** ← Data producers, Data producers — **LANL** → **RACER database** → **Transparent processes** • Stakeholder input • Risk evaluations • Risk-reduction options → **Website** → **Public and all data users**

Human Performance and Highly Reliable Organizations

The philosophy of human performance is an approach to understanding human error that entails more than reading accident reports and analyzing spreadsheets.

Eliminating human error may appear to be a simple process—if workers paid more attention to their tasks, they would be safer. However, eliminating error is neither simple nor easy. More important, fixating on error removal may, in fact, be the wrong approach to creating a safer, more-effective work environment. Let's face it, errors happen; they are part of the human condition, an invaluable component in the development of improved programs and practices. Learning from inconsequential mistakes and basic human error, rather than sweeping them under the rug of zero-tolerance management edicts, enables a work environment that is conducive to preventing catastrophic failure.

Errors are information, indicators of weakness within a facility's operations. Errors show us where our systems are flawed and where our processes are faulty. Within the context of continually trying to improve processes, errors guide our focus, direction, and efforts in terms of familiarizing, training, qualifying, rewriting, and rethinking. Error may be our most important ally in fully understanding the cause and effect of the human fallibility factor in the workplace.

Highly reliable organizations spend much time, energy, resources, and money trying to improve worker safety behavior. All too often, this single-minded approach, centered on fixing the system by fixing the worker, creates the appearance of a work environment that is completely intolerant of human error. It also implies, incorrectly, that workers are the problem, when in fact, workers—and the

missteps they encounter—are vital to solving an organization's insufficiencies. Furthermore, this approach may foster the belief among the work force that (1) management will blow errors out of proportion and (2) minor incidents should be covered up rather than reported. This kind of thinking is dangerous and has potentially intolerable consequences.

Errors are information that can show us how to improve.

Laboratory management now recognizes that many consistently and dutifully sent messages to our workers, however well intentioned, may have been wrong. We can never overemphasize the importance of safety. Yet if we design safety systems that assume all workers will be completely on their A-game 100% of the time, we will build safety systems that are inherently prone to failure. A truly fail-safe system must include the potential for human error.

Principles of Human Performance

Human performance as a facet of organizational assessment comes to DOE from the Institute for Nuclear Performance Operations (INPO)—a consortium of America's nuclear power production facilities that has studied safety performance and behavior at their facilities for the last 15 years.

The nuclear power industry and INPO began this journey of discovery and analysis before most other large-scale industries for which safety is a primary concern. Traditionally, the question has been "How can we keep our workers safe within our facilities?" But after Three Mile Island, the question became "How can we keep our facilities safe from our workers?" On the surface, this question may seem to

represent a "blame the workers" mentality, when in fact it accurately recognizes a natural potential for human error. It is the right question to ask to ensure safety for all.

Without doubt, the process of reframing such a valid and important question about worker safety led to an evaluation of the nuclear power industry's perceptions of safety issues. As a result, INPO devised the following revolutionary set of key human performance principles that reflects the industry's realigned safety, quality, and performance directives:

1. People are fallible—even the best make mistakes.

2. Error-likely situations are predictable, manageable, and preventable.

3. Individual behavior is influenced by organizational processes and values.

4. People achieve high levels of performance based largely on the encouragement and reinforcement received from leaders, peers, and subordinates.

5. Events can be avoided by understanding the reasons mistakes occur and applying lessons learned from past events.

These principles represent a salient approach to the realities of human performance. How should these ideas affect the way our Laboratory organizations deal with safety, quality, security, and production issues?
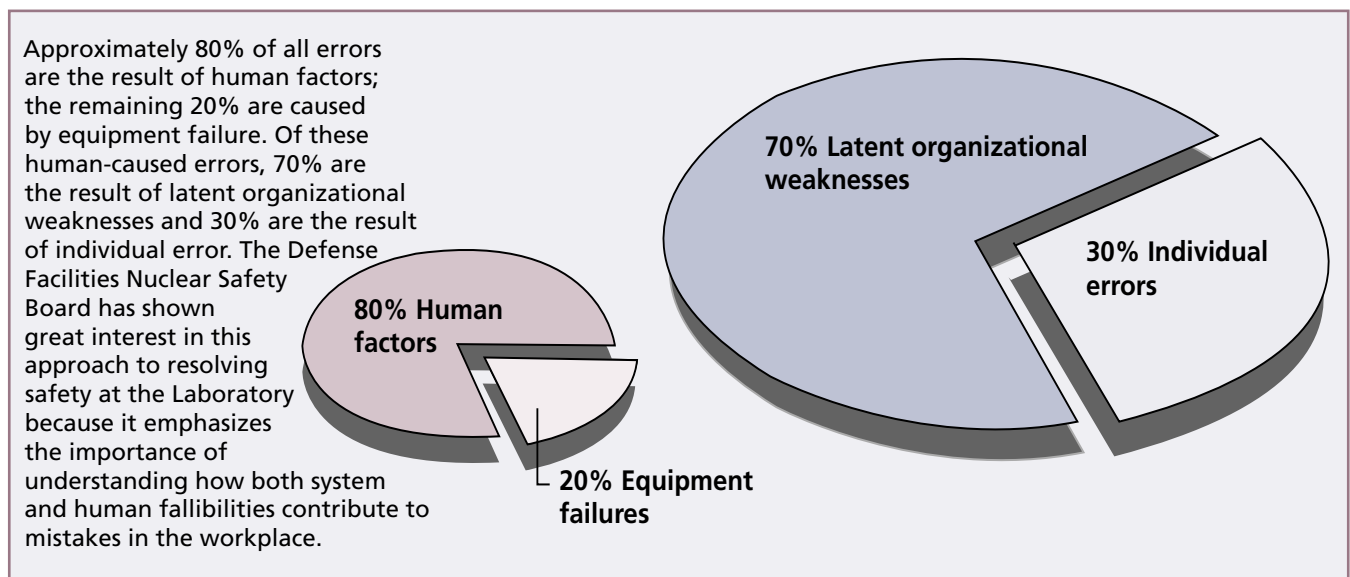
Reliable Organizations

Many highly reliable Laboratory organizations successfully include activities and environments that are inherently dangerous. To conduct their work safely, these institutions expect the unexpected and quickly adapt when the environment changes. Equally important, every employee accepts responsibility for reliability.

We know that workers are motivated, limited, encouraged, and controlled by the organizations they make up. Asking workers to be more careful disregards this reality, denies the validity of the principles of human performance, and disassociates workers from constructive involvement in developing solutions to safety-related concerns. Only through working together as a team and collectively recognizing that mistakes occur at any and all levels of every organization can we design and implement procedures that create a safe and productive workplace. NWJ

Point of contact:
Todd Conklin, 665-8650, bigtodd@lanl.gov

Approximately 80% of all errors are the result of human factors; the remaining 20% are caused by equipment failure. Of these human-caused errors, 70% are the result of latent organizational weaknesses and 30% are the result of individual error. The Defense Facilities Nuclear Safety Board has shown great interest in this approach to resolving safety at the Laboratory because it emphasizes the importance of understanding how both system and human fallibilities contribute to mistakes in the workplace.

80% Human factors

20% Equipment failures

70% Latent organizational weaknesses

30% Individual errors

Los Alamos and its sister laboratories must develop logical, affordable plans for interim forms of deterrence, e.g., extending stockpile life and ensuring reliable, responsive designs.

As we work to resolve key questions about pit lifetimes, we must provide responsive technical solutions that, in the short term, demonstrate strength that effectively deters the proliferation of nuclear materials and designs. Once the nation determines its long-term deterrence policy, the nuclear materials infrastructure we have built at Los Alamos can respond as needed with plutonium science capability and interim pit capacity.

Currently, we are maintaining a shrinking stockpile of nuclear weapons designed for a superpower cold war and with an average age of nearly 30 years—well beyond their original design lifetimes. As the nation further reduces the stockpile, Los Alamos must help answer questions about what types of weapons are right for this smaller stockpile and radically different global threats. The Laboratory can strengthen the nation's security posture by further developing a responsive infrastructure—a nuclear weapons complex able to meet a wide range of challenging technical goals.

Los Alamos is able to solve complex technical problems as they emerge in a rapidly changing security environment. Our capabilities in nuclear materials allow us to lead the nation in developing nuclear fuels and reactors for next-generation space travel, recycled mixed-oxide fuels that minimize proliferation risks while providing long-term energy solutions, and innovative materials that meet future weapon requirements. The Laboratory has the people and the multidisciplinary facilities to meet national needs in actinide science: from first-principles research and development and complex modeling and simulation to deployment of hardware that demonstrates pilot-scale manufacturing and environmental processes.

Other national laboratories and the National Nuclear Security Administration's manufacturing complex continue to rely on us to suggest and promote creative technical solutions in nuclear materials and many other technical fields. Such solutions grow out of strong, close relationships among those engaged in the national security enterprise. These partnerships of mutual reliance are the key to effective, affordable stockpile stewardship and to realistic manufacturing solutions upon which long-term nuclear deterrence depends.

So to those who want to come to Los Alamos and to those already fortunate enough to be here, I ask you to provide the commitment needed for continued nuclear deterrence and a stronger overall national security posture. With pride in our traditions and what we have accomplished, we will answer the call for technical leadership as trusted, innovative team members of the nuclear weapons complex. NWJ

A BACKWARD GLANCE

Robert Bacher: Taking a Stand for Science

By early 1943, General Leslie R. Groves and J. Robert Oppenheimer had finalized plans to establish a secret research laboratory in the mountains of northern New Mexico. Groves assumed that a US Army officer would operate the lab, with all the scientists accepting commissions. Oppenheimer, who stood ready to accept his commission as a lieutenant colonel, raised no objections. In fact, he even ordered several uniforms. But many scientists, with physicist Robert F. Bacher at the fore, objected to military control.

During the 1930s, Bacher had established himself as one of the leading physicists of his generation, working with many prominent scientists including Samuel Goudsmit, Enrico Fermi, and Hans Bethe. When World War II broke out, Bacher was asked to lead a division at the Massachusetts Institute of Technology's Radiation Laboratory (RadLab), where he played an important role in developing

Atomic Energy Commissioners (l to r) Robert F. Bacher, David E. Lillenthal (chairman), Sumner T. Pike, William W. Wamack, and Lewis L. Strauss.

early radar technology. The experience he gained as an administrator, coupled with his scientific expertise, made him the ideal candidate to head Oppenheimer's Experimental Physics Division. But the specter of military control remained an insurmountable stumbling block to Bacher.

Oppenheimer realized Bacher's incredible value, stating, "His qualifications, and his historical connection [with our] project, make him our first choice, in priority and in importance." As such, he arranged for Bacher and fellow opposition leader I. I. Rabi to meet with Manhattan Project leaders to discuss military control. Bacher's position was simple: "Science does not mix with military management and while I do not object to joining the army I would at present not do so as a scientist."

General Groves eventually conceded, allowing UC to run Los Alamos. The relationship between the Manhattan Project and UC was formalized in a contract, signed April 20, 1943.

Bacher soon joined the project, but warned that his letter of acceptance would become his letter of resignation effective the day the army took over. Civilians have operated the Laboratory ever since Bacher and a handful of his colleagues chose to take a stand for science more than 60 years ago.

Bacher's contribution to science continued after the war. He received the President's Medal for Merit in 1946 and was one of the first members of the Atomic Energy Commission. During the Eisenhower administration, Bacher was a member of the US Science Advisory Committee.

He joined the Caltech faculty in 1949. At Caltech, he headed the physics department, also serving as vice president and provost. He also helped initiate the Owens Valley Radio Observatory, a leading radio astronomy facility, and was president of the American Physical Society and of the International Union of Pure and Applied Physics.
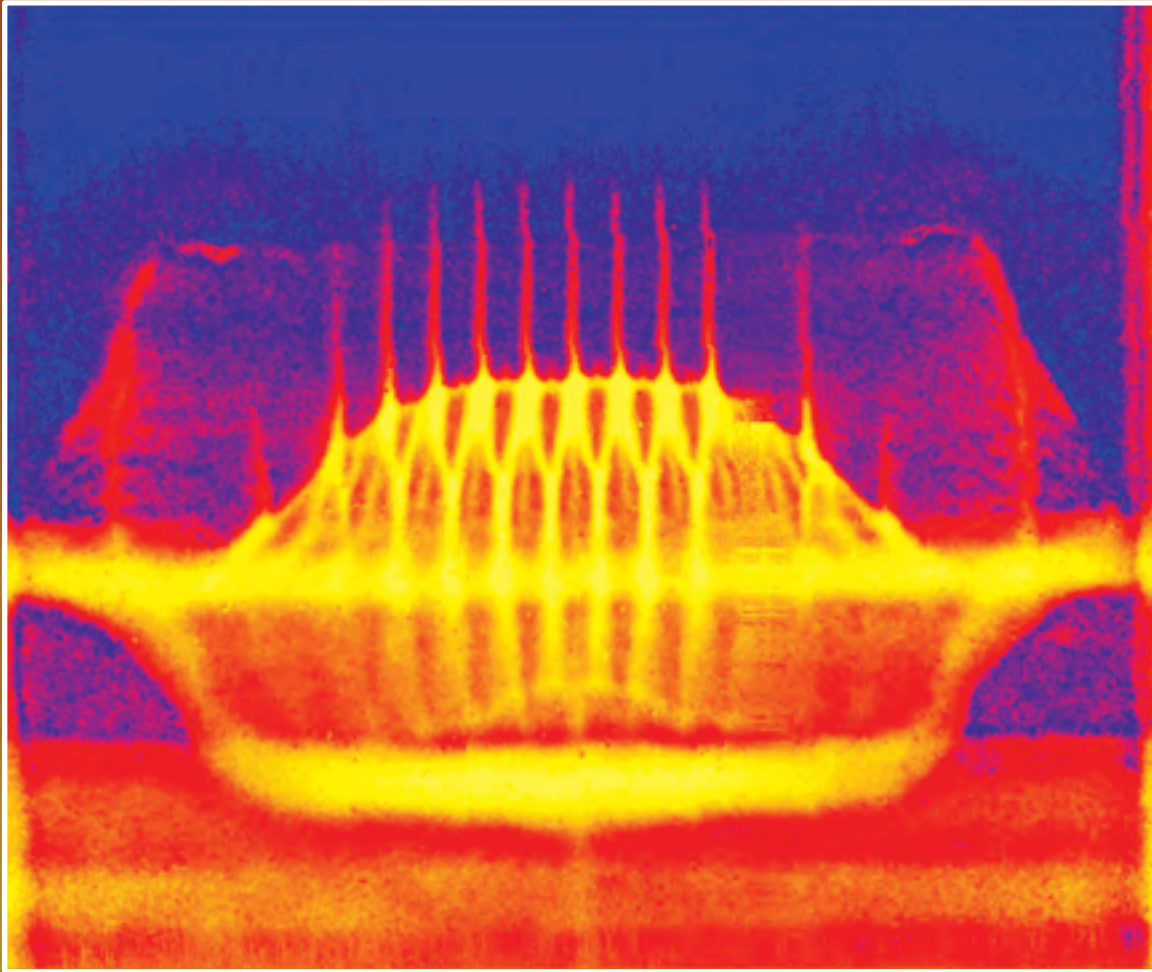
Bacher died in November 2004 at his home near Santa Barbara. NW

Point of contact:
Alan B. Carr, 664-0870, abcarr@lanl.gov